

# Four New Compact Triply Eclipsing Triples found with *Gaia* and *TESS*

Donát R. Czavalinga,<sup>1,2\*</sup> Tamás Borkovits,<sup>1,2,3,4,5</sup> Tibor Mitnyan,<sup>1,2</sup> Saul A. Rappaport,<sup>6</sup> András Pál<sup>3</sup>

<sup>1</sup> Baja Astronomical Observatory of University of Szeged, H-6500 Baja, Szegedi út, Kt. 766, Hungary

<sup>2</sup> HUN-REN-SZTE Stellar Astrophysics Research Group, H-6500 Baja, Szegedi út, Kt. 766, Hungary

<sup>3</sup> Konkoly Observatory, Research Centre for Astronomy and Earth Sciences, H-1121 Budapest, Konkoly Thege Miklós út 15-17, Hungary

<sup>4</sup> ELTE Gothard Astrophysical Observatory, H-9700 Szombathely, Szent Imre h. u. 112, Hungary

<sup>5</sup> HUN-REN-ELTE Exoplanet Systems Research Group, H-9700 Szombathely, Szent Imre h. u. 112, Hungary

<sup>6</sup> Department of Physics, Kavli Institute for Astrophysics and Space Research, M.I.T., Cambridge, MA 02139, USA

Accepted XXX. Received YYY; in original form ZZZ

## ABSTRACT

This paper presents a comprehensive analysis of four triply eclipsing triple star systems, namely TIC 88206187, TIC 14839347, TIC 298714297, and TIC 66893949. The four systems with third-body eclipses were found in the *TESS* lightcurves from among a sample of  $\sim 400$  matches between known eclipsing binaries and the *Gaia* DR3 Non-Single Star (NSS; [Gaia Collaboration 2022](#); [Pourbaix et al. 2022](#)) solution database. We combined photometric lightcurves, eclipse timing variations, archival spectral energy distributions, and theoretical evolution tracks in a robust photodynamical analysis to determine the orbital and system parameters. The triples have outer periods of 52.9, 85.5, 117, and 471 days, respectively. All dozen stars have masses  $\lesssim 2.6 M_{\odot}$ . The systems are quite flat with mutual inclination angles between the inner and outer orbital planes that are all  $\lesssim 4^{\circ}$ . The outer mass ratios ( $q \equiv M_3/M_{\text{bin}}$ ) range from 0.39–0.76, consistent with our earlier collection of compact triply eclipsing triples. TIC 88206187 exhibits a fractional radius of the outer tertiary component ( $r_B \equiv R_B/a_{\text{out}}$ ) exceeding 0.1 (only the third such system known), and we consider its future evolution. Finally, we compare our photodynamical analysis results and the orbital parameters given in the *Gaia* DR3 NSS solutions, indicating decent agreement, but with the photodynamical results being more accurate.

**Key words:** binaries:eclipsing – binaries:close – stars:individual: TIC 14839347, TIC 66893949, TIC 88206187, TIC 298714297

## 1 INTRODUCTION

Triply eclipsing triple star systems are outstanding objects in which to study the properties and dynamics of multistellar systems. These are triple systems in which the inner binary eclipses the tertiary star, or vice versa, during the course of their outer orbit. The outer orbital periods range from a month to a year or two, and therefore dynamical interactions can usually be observed within the duration of a PhD study. Furthermore, even in the absence of radial velocity (RV) observations, readily available spaced-based photometric observations, such as with *Kepler* ([Borucki et al. 2010](#)) or *TESS* ([Ricker et al. 2015](#)) can yield precise eclipse timing measurements, as well as the photometry of the third-body eclipses. These can be combined with the archival spectral energy distribution, and processed in a comprehensive spectro-photodynamical analysis to yield a full set of accurately determined stellar and orbital parameters for the system. In terms of the spatial configuration of the system, this analysis can provide such quantities as the ratio of orbital periods, the orbital eccentricities, and the mutual inclination of the two orbits. In turn, these quantities play a crucial role in the long-term evolution of the whole system. These are therefore excellent laboratories for testing theories regard-

ing the formation, evolution and final evolutionary states of multi-star systems.

The first such system was discovered in *Kepler* data by [Carter et al. \(2011\)](#), and the second one followed very shortly thereafter ([Derekas et al. 2011](#)). Within a few years, more than a dozen publications had reported the discovery of 15 more similar objects, among them the first detections using other observing facilities than *Kepler*, including *CoRoT* ([Hajdu et al. 2017](#)) and OGLE ([Hajdu et al. 2022](#)). Since then, *TESS* observations have accelerated the search for these objects and have led the way in such studies. [Borkovits et al. \(2020b\)](#) reported the first identification and analysis of a triply eclipsing triple based on *TESS* data, and in less than three years since then, 20 additional similar objects have been identified and analyzed in detail ([Mitnyan et al. 2020](#); [Borkovits et al. 2022](#); [Powell et al. 2022](#); [Rappaport et al. 2022, 2023](#)). That means, thanks to *Kepler* and then nowadays *TESS*, the discovery of triply eclipsing triples has become more or less routine, and the numbers of known triply eclipsing triple systems have been steadily growing.

In our previous work ([Czavalinga et al. 2023](#)), we utilized the *Gaia* Data Release 3 (DR3; [Gaia Collaboration et al. 2023](#); [Babusiaux et al. 2023](#)) Non-Single Star (NSS; [Gaia Collaboration 2022](#); [Pourbaix et al. 2022](#)) solutions to search for tertiary stars in eclipsing binary (EB) systems that had previously been reported in the literature. *Gaia* DR3 provides a unique opportunity to search for close hierarchical

\* E-mail: czdonat@titan.physx.u-szeged.hu

triple stars across the entire sky based on long-term astrometric and spectroscopic observations. If we compare the eclipsing period with the period obtained from the *Gaia* NSS solutions, and the period ratio is higher than 5, we can infer that the object is likely a triple-star system candidate with the inner period being that of the EB and the outer period of the tertiary star the one determined by *Gaia*'s NSS solutions (see Czavalinga et al. 2023, for details). Using this method, we identified 403 potential compact hierarchical triple-star system candidates among  $\sim 1$  million known EBs, including four newly identified triply eclipsing triples. Here we provide a detailed analysis of the latter four systems. In Section 2, we describe the observational data and the methods utilized for the discovery and validation of the corresponding objects. In Section 3, we construct a photodynamical model for each system, and then in Section 4, we give a detailed discussion of the resulting models. In Section 5, we compare the orbital parameters from our photodynamical models with those from the *Gaia* NSS solutions, and finally we summarize our findings in Section 6.

## 2 DISCOVERY AND OBSERVATIONS

### 2.1 TESS observations

To validate the triple nature of our candidate systems we started by constructing a *TESS* photometric lightcurve (LC) for each one. Our aim was to search for eclipse timing variations (ETVs) and possible third-body eclipses in the LC. After downloading all the available Full-Frame Images (FFIs) from the MAST portal<sup>1</sup>, we applied the same convolution-aided image subtraction photometry pipeline based on FITSH (Pál 2012) along with the same detrending process based on the WOTAN (Hippke et al. 2019) and lightkurve (Lightkurve Collaboration et al. 2018) Python packages that we used in our previous paper (see details in Czavalinga et al. 2023).

We identified six LCs with potential extra third-body eclipses. Two of them had already been discovered by other teams, with one system being HD 181068, the second triply eclipsing triple found in *Kepler* observations (Derekas et al. 2011), and the other one being TIC 229785001 recently analyzed in detail by Rappaport et al. (2023). The remaining four systems were completely unknown in the literature. These are as follows:

TIC 14839347 was observed by *TESS* in Sectors 14, 15, 41, and 55. We found a well-defined third-body eclipse in Sector 41, and then, after making use of the outer period from the *Gaia* NSS solution, we additionally found two very shallow secondary eclipses in Sectors 14 and 55 (see upper left panel of Fig. 1).

TIC 66893949 was observed in Sectors 15, 41, and 55. In Sector 15, we identified an extra dip in the LC, which we interpreted as third-body eclipse. No eclipses occurred in Sector 41, but we observed two extra eclipsing events with different depths in Sector 55 (upper right panel of Fig. 1). We note that recently Rowan et al. (2023) also independently discovered this object as a triply eclipsing triple, but they have not analyzed the system in any detail.

TIC 88206187 was observed by *TESS* in Sectors 19 and 59. We discovered a very deep and long, flat bottomed eclipse in the middle of Sector 19. The source also produced another, similarly long in duration but much shallower, third-body eclipse in Sector 59 (lower left panel of Fig. 1).

Finally, TIC 298714297 was observed in Sectors 15, 55, and 56 by *TESS*. We found evidence for one third-body eclipse in Sector 55,

accompanied by what are likely prominent, stellar-activity induced variations in the LC (lower right panel of Fig. 1).

For the ETV calculation, we applied the same process as in our previous paper (Czavalinga et al. 2023), and that is described in detail in Borkovits et al. (2015). In short, we fitted template polynomials to both the primary and secondary eclipses in the phase-folded, binned LC of each system. The mid-eclipse times were thereby determined for each orbital cycle. We list the determined individual mid-eclipse times in Tables A1–A4 separately for all the four systems.

### 2.2 ASAS-SN, ATLAS observations

We looked up all four triply eclipsing triples in the ASAS-SN (Shappee et al. 2014; Kochanek et al. 2017) and ATLAS (Tonry et al. 2018; Smith et al. 2020) archives. All four systems have good data in the ASAS-SN archives, and two have useful data in the ATLAS archives (TIC 298714297 and TIC 66893949 are too bright for ATLAS). We readily see the EB LC in the archival data for all four systems.

After we determine an accurate EB period for data that span of order a decade, we remove the EB LC by fitting for, and then subtracting out, between 50 and 100 orbital harmonics. This allows for a more sensitive BLS search (Box Least Squares; Kovács et al. 2002) for the eclipses of the outer orbit.

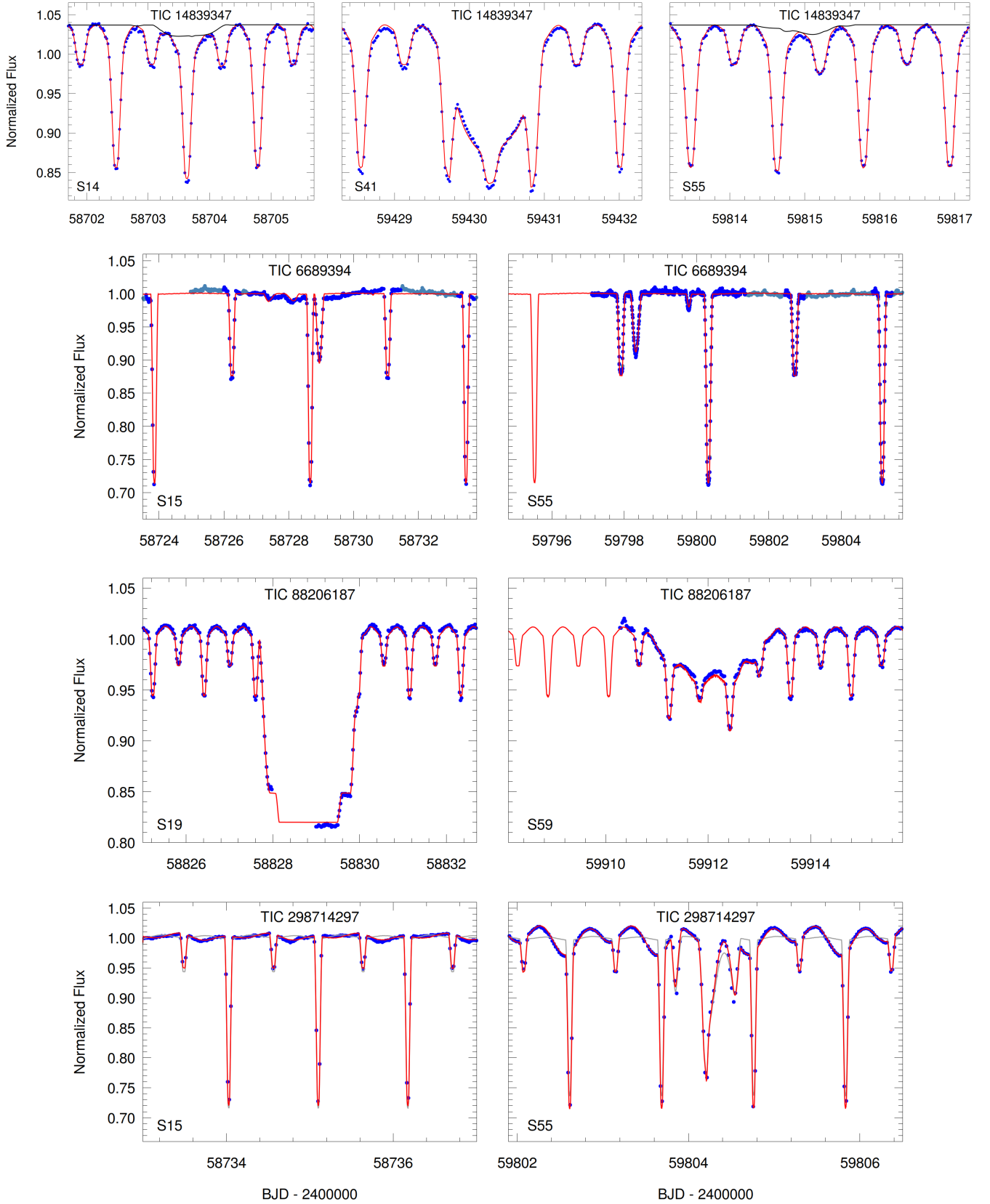
For TIC 66893949 and TIC 298714297 (with outer periods of 470.6 and 118.6 days, respectively) there are insufficient archival data, and too few outer eclipses observed, to make a statistically significant detection of the outer eclipses. However, for TIC 14839347 and TIC 88206187, the outer periods of 85.47 days and 52.84 days, respectively, were robustly detected in a combination of the ASAS-SN and ATLAS data. The results are shown in Figs. 2 and 3, respectively. In the case of TIC 88206187, Fig. 3 shows a shallow but clear secondary outer eclipse. The phasing of the two outer eclipses yields  $e_{\text{out}} \cos \omega_{\text{out}} = 0.003 \pm 0.005$ , with an implication that the outer orbit is likely fairly circular.

## 3 PHOTODYNAMICAL ANALYSIS

Similar to other *TESS*-discovered triply eclipsing triple stars, we carried out a joint, simultaneous LC, ETV curve and spectral energy distribution (SED) analysis with the software package LIGHTCURVEFACTORY. The software package itself, and the consecutive steps of the complex analysis, were described in several papers, e.g., in Borkovits et al. (2020a, 2022); Rappaport et al. (2023) and, hence, we will not repeat the details here, but rather restrict ourselves to some particular notes about the current, specific systems.

Our analyses are mainly based on the *TESS* LCs, which were processed in the manner described in Sect 2.1. In contrast to the vast majority of our former analyses of triple and quadruple systems, in the case of 3 of the 4 systems reported here, we did not restrict our analyses only to the narrow regions of the inner and outer eclipses, dropping out the majority of the out-of-eclipse portions of the LCs, but rather we kept the complete *TESS* time series. The reason is that, apart from the somewhat wider 4.8-day inner EB in TIC 66893949, the other three, much more compact inner EBs, display significant ellipsoidal light variations in the out-of-eclipse LC sections, which we found to be worthwhile to retain for the analysis. Moreover, we note the special case of TIC 298714297, in which the LC exhibits further remarkable rotational variations with periods similar to the eclipsing period of the inner EB. We modelled these variations simultaneously with the full, eclipsing LC solution (but separately for

<sup>1</sup> <https://mast.stsci.edu/>

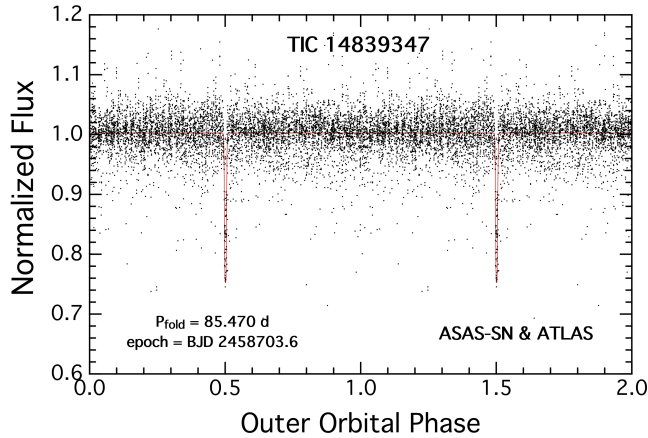
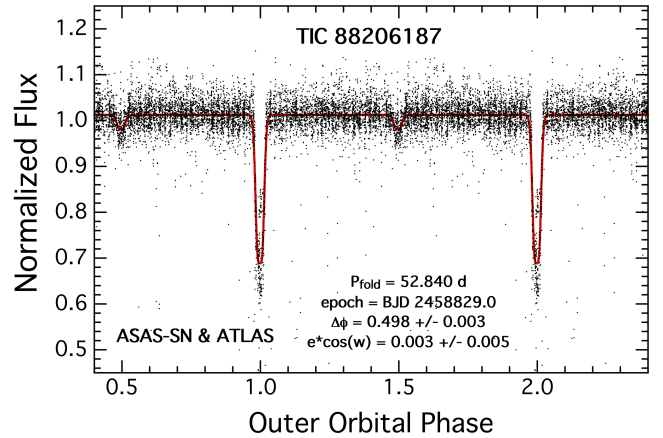


**Figure 1.** Sections of *TESS* LCs with third-body eclipse events for each of the four triple systems. The blue points are the *TESS* observations, while the overplotted smooth red curves are the models from the photodynamical fit (see Sect. 3). In the left and right upper panels (the two very shallow secondary outer eclipses of TIC 14839347), the additional black lines represent just the flux occultations of the giant tertiary component as the EB passes in front of it. In the second row, the lighter blue points in the out-of-eclipse regions of TIC 6689394 were omitted from the photodynamical fits to save computation time. In the case of TIC 298714297 (bottom row) the gray curve displays the pure EB model (without the Fourier-modeled rotational distortions).

**Table 1.** Main parameters of the four systems from the literature.

Parameter	TIC 14839347	TIC 66893949	TIC 88206187	TIC 298714297
<i>Gaia</i> Source ID <sup>a</sup>	2058085351143518464	1870771652581668352	207943285475761280	1849392443551822848
RA <sup>a</sup> [deg]	306.408	311.711	82.739	324.463
DEC <sup>a</sup> [deg]	37.895	36.352	44.803	29.474
T <sup>b</sup> [mag]	12.2117 ± 0.0448	11.6134 ± 0.0101	11.8518 ± 0.0078	10.8136 ± 0.0069
G <sup>a</sup> [mag]	13.070626 ± 0.002975	11.9993 ± 0.0002	12.478771 ± 0.002864	11.542984 ± 0.003035
G <sub>bp</sub> <sup>a</sup> [mag]	13.866420 ± 0.004369	12.2891 ± 0.0008	13.006023 ± 0.003710	12.203759 ± 0.004678
G <sub>rp</sub> <sup>a</sup> [mag]	12.175914 ± 0.005246	11.5470 ± 0.0005	11.783351 ± 0.004393	10.743742 ± 0.004989
B <sup>c</sup> [mag]	14.837 ± 0.048	12.47 ± 0.255	13.403 ± 0.275	13.309 ± 0.399
V <sup>c</sup> [mag]	13.807 ± 0.149	12.082 ± 0.057	12.794 ± 0.069	11.584 ± 0.138
g <sup>c</sup> [mag]	14.211 ± 0.016	12.408 ± 0.000	13.007 ± 0.220	12.493 ± 0.040
r <sup>c</sup> [mag]	13.176 ± 0.033	12.058 ± 0.000	12.487 ± 0.072	11.529 ± 0.045
i <sup>c</sup> [mag]	12.562 ± 0.019	11.869 ± 0.000	12.135 ± 0.084	11.055 ± 0.051
J <sup>d</sup> [mag]	10.81 ± 0.021	11.004 ± 0.021	10.828 ± 0.022	9.717 ± 0.028
H <sup>d</sup> [mag]	10.231 ± 0.018	10.737 ± 0.017	10.351 ± 0.021	9.092 ± 0.034
K <sup>d</sup> [mag]	9.999 ± 0.016	10.697 ± 0.016	10.206 ± 0.016	8.965 ± 0.02
W1 <sup>e</sup> [mag]	9.827 ± 0.023	10.685 ± 0.023	10.099 ± 0.023	8.877 ± 0.023
W2 <sup>e</sup> [mag]	9.857 ± 0.02	10.72 ± 0.021	10.129 ± 0.02	8.878 ± 0.02
W3 <sup>e</sup> [mag]	9.673 ± 0.088	10.666 ± 0.099	10.011 ± 0.062	8.752 ± 0.024
W4 <sup>e</sup> [mag]	7.836 ± 0.191	9.015 ± NaN	8.67 ± 0.36	8.82 ± 0.378
T <sub>eff</sub> <sup>a</sup> [K]	-	5883 ± 27	-	5498 ± 121
Distance <sup>f</sup> [pc]	1970 <sup>+48</sup> <sub>-41</sub>	587 <sup>+9</sup> <sub>-7</sub>	2490 <sup>+96</sup> <sub>-78</sub>	111.9 <sup>+0.7</sup> <sub>-0.7</sub>
E[B - V] <sup>c</sup> [mag]	0.772 ± 0.065	0.03929 ± 0.0124	0.2585 ± NaN	0.009 ± 0.00595
μ <sub>α</sub> <sup>a</sup>	-2.657 ± 0.011	14.4171 ± 0.0202	0.720 ± 0.015	-28.768 ± 0.044
μ <sub>δ</sub> <sup>a</sup>	-7.034 ± 0.012	-15.2782 ± 0.0241	-2.416 ± 0.011	-58.138 ± 0.036
RUWE <sup>a</sup>	1.221	1.9273869	0.905	3.162
NSS model <sup>a</sup>	SB1	Orbital	SB1	Orbital
P <sub>binary</sub> <sup>g</sup> [days]	1.154060 <sup>+0.000050</sup> <sub>-0.000052</sub>	4.805309 <sup>+0.000004</sup> <sub>-0.000005</sub>	1.184592 <sup>+0.000055</sup> <sub>-0.000063</sub>	1.072891 <sup>+0.000010</sup> <sub>-0.000019</sub>
P <sub>triple</sub> <sup>g</sup> [days]	85.530 <sup>+0.017</sup> <sub>-0.017</sub>	471.03 <sup>+0.10</sup> <sub>-0.07</sub>	52.922 <sup>+0.041</sup> <sub>-0.039</sub>	117.24 <sup>+0.36</sup> <sub>-0.31</sub>

Notes. '-' means that the value is not available (a) - *Gaia* DR3 (Gaia Collaboration et al. 2023), coordinates: ICRS J2016.0; (b) - *TESS* Input Catalog V8.2 (Paegert et al. 2021); (c) - AAVSO Photometric All Sky Survey (APASS) DR9 (Henden et al. 2015); (d) - 2MASS All-Sky Catalog (Skrutskie et al. 2006); (e) - ALLWISE Data Release (Cutri et al. 2021); (f) - (Bailer-Jones et al. 2021); (g) - parameters from this paper

**Figure 2.** Folded outer orbit of TIC 14839347.**Figure 3.** Folded outer orbit of TIC 88206187.

Sectors 15 and 55-56), with the use of additional fits of harmonic functions in the manner described, e.g., in Borkovits et al. (2018, 2021).

As usual, we fit the ETV curves of the four EBs simultaneously with their LCs. As our literature search did not turn up any additional previously recorded eclipse times, our ETV curves were restricted to only those times that we determined from the *TESS* observations themselves.

Due to the lack of publicly available RV timeseries for any

of the four currently investigated systems, with the exception of TIC 14839347, we used a combination of (i) observed composite SED values (tabulated from the available catalog passband magnitudes, and listed in Table 1) and (ii) pre-computed, tabulated PARSEC isochrones (Bressan et al. 2012) to find stellar masses and corresponding effective temperatures, as well. The use of PARSEC isochrone-based SED analysis for this purpose was explained in Borkovits et al. 2020a, while a comparison of the accuracy and efficiency of such an astrophysical model-dependent analysis with



the classical, astrophysical model-independent analysis (the latter of which is based on RV data), was carried out and discussed in [Borkovits et al. 2022](#).

In the case of one of the four systems, TIC 14839347, our preliminary analysis run, however, revealed a situation where the secondary is fairly low in mass, but large enough to fill or nearly fill its Roche lobe. We therefore suspect that the secondary star in TIC 14839347 may have already transferred a portion of its envelope to the (current) primary star. As a consequence, for this triple we cannot use this proxy method because the precomputed PARSEC evolution grids are valid only for single stars, i.e., for such binary components which have not previously exchanged mass. Therefore, in the case of this particular triple, we followed an iterative method as follows. First, we carried out LIGHTCURVEFACTORY fitting, excluding the SED analysis section. In such a way, we obtained strong constraints for the relative (or, fractional) radii of the three stars, as well as their temperature ratios. Then, using these relative quantities, as well as the *Gaia* EDR3 derived distance ([Bailer-Jones et al. 2021](#)), we made an independent SED analysis without the use of any astrophysical pre-assumptions, with a slightly modified version of the method described in [Rappaport et al. \(2022\)](#), Sect. 3. In this way, we obtained likely mass and temperature ranges for the three constituent stars. Then we used the SED-determined values for the mass of the primary of the inner binary ( $m_{Aa}$ ) and the effective temperature of the tertiary ( $T_B$ ) with their statistical uncertainties as Gaussian priors, and reiterated the whole simultaneous LC and ETV curve fitting procedure with LIGHTCURVEFACTORY. With this iterative procedure, we were able to find the system geometry and dynamics robustly, while also inferring the physical properties of the constituent stars at a reasonable level of accuracy.

In regard to TIC 14839347, we also had to introduce some further modification to the light-curve fitting part of the complex analysis. We found that, in this case, the reflection/irradiation effect gives a significant contribution to the LC of the inner EB. Hence, we “switched on” this effect for the modeling. First we set the bolometric albedos according to the theoretically expected values of  $A = 1.0$  and  $0.5$  for the primary (Aa) and secondary stars (Ab), (i.e., radiative and convective envelopes) respectively. We found, however, that the fit becomes distinctly better when one sets  $A_{Ab} \approx 0.8$ . For this reason, finally we decided to adjust, as an exception to our usual approach, the bolometric albedos and gravity darkening exponents ( $\beta$ ) for these two stars.

Finally we note the fact that none of the four investigated triples is a ‘tight’ system (the outer-to-inner period ratios,  $P_{out}/P_{in}$  are somewhat large, ranging from 45 for TIC 88206187, to 109 TIC 298714297) and, hence, one cannot expect significant third-body perturbations which would produce significant departures from simple Keplerian motions. On the other hand, considering the fact that the third-body eclipses are extremely sensitive to the current system geometry, similar to our former analyses (where much tighter triples were analysed) we integrated the motion of the three stellar components numerically, instead of approximating the motion with the superposition of two Keplerian orbits. The numerical integrator built into LIGHTCURVEFACTORY is a seventh order Runge-Kutta-Nystrom integrator. This integrator provides the gravitationally (pure Newtonian two- and three-body terms), tidally (within the framework of the equilibrium tide model) and, optionally, the relativistically perturbed Cartesian Jacobian coordinates (and velocities) for each observational instant. A detailed description of the integrator itself, and its implementation in the photodynamical software package can be found in [Borkovits et al. \(2004, 2019a,b\)](#).

We initialized and ran several MCMC chains for each of the four

triple systems. The best fit parameters (median values of the posteriors), their  $1 - \sigma$  uncertainties, as well as several derived parameters, are tabulated in Tables 2 and 3. Here we note, that while most of the given derived parameters (e.g., the semi-major axes, radial velocity amplitudes, bolometric luminosities, etc.) do not require any further explanations, we discuss briefly the calculations and significances of the different apsidal and nodal motion parameters, tabulated in between the orbital elements and the stellar parameters.

We give the theoretical apsidal motion periods both in the observational and the dynamical frames of reference ( $P_{apse}$  and  $P_{apse}^{dyn}$ ). While the formulae for their calculations, from the initial osculating orbital elements at each accepted MCMC trial step, are discussed in detail in Sect. 6.3 of [Kostov et al. \(2021\)](#), here we emphasize only the fact that the observational and dynamical apsidal motions and, hence, their timescales are substantially different. From an observational point of view, what is significant is the revolution of the argument of periastron in the observational frame of reference.<sup>2</sup> This revolution manifests itself, e.g., in the periodic, quasi-sinusoidal and anticorrelated shifts of the primary and secondary eclipses, in the case of eccentric EBs. In contrast to this, the revolution of the argument of pericenter in the dynamical frame<sup>3</sup> cannot be observed directly, however, this dynamical argument of periastron and, hence, the dynamical-frame apsidal motion are significant for dynamical studies, as this parameter is one that occurs in the perturbation equations. The observable-frame apsidal motion, in general, is a non-linear combination of the dynamical-frame apsidal motion and the (dynamical) nodal regression, and hence, their periods (i.e.,  $P_{apse}$  and  $P_{apse}^{dyn}$ ) may be substantially different (see, e.g., [Borkovits et al. 2015](#) for further details). Note also, that besides the apsidal motion and nodal regression ( $P_{node}^{dyn}$ ) periods, we give separately the three components of the apsidal advance rates (classical tidal,  $\Delta\omega_{tide}$ ; general relativistic,  $\Delta\omega_{GR}$ ; and dynamical third-body,  $\Delta\omega_{3b}$ , respectively) for one orbital revolution of the inner and outer orbits, respectively. These contributions are calculated in the dynamical frame of reference.

Finally, note that the third-body eclipse sections of the model LCs from the best-fit complex photodynamical solutions are plotted in Fig. 1, while the model ETV curves of the best-fit solutions are shown in Figs. 4–7. We briefly discuss our results for each system separately in Sect. 4.

## 4 DISCUSSION

### 4.1 TIC 14839347

As was mentioned above, the analysis of this triple system had to be carried out iteratively, and with extra care. We adopted  $m_{Aa} = 2.50 \pm 0.13 M_{\odot}$  and  $T_B = 5000 \pm 200$  K for the mass of the primary and effective temperature of the tertiary, from the separate SED analysis. The inner mass ratio was found to be as low as  $q_{in} = 0.25 \pm 0.02$ ,

<sup>2</sup> The basic plane of the observational reference frame is the tangential plane of the sky, which is perpendicular to the line of sight to the target as seen by the observer. The argument of pericenter in this frame is the angle measured from one of the intersections of the orbit and the nodal line of this tangential plane and the orbital plane, to the pericenter point, along the orbit.

<sup>3</sup> The basic plane of the dynamical reference frame is the invariable plane of the triple system, i.e., the plane whose normal is parallel to the constant total angular momentum of the triple. The argument of pericenter in this frame is measured from one of the intersections of the orbit and the nodal line of this invariable plane and the orbital plane, to the pericenter point, along the orbit.

**Table 2.** Orbital and astrophysical parameters of TICs 14839347 and 66893949 from the joint photodynamical *TESS*, ETV, SED and PARSEC isochrone solution. Note that the orbital parameters are instantaneous, osculating orbital elements and are given for epoch  $t_0$  (first row).

	TIC 14839347			TIC 66893949		
	orbital elements					
	subsystem			subsystem		
	Aa–Ab	A–B		Aa–Ab	A–B	
$t_0$ [BJD - 2400000]	58 683.0			58 711.0		
$P$ [days]	$1.154060^{+0.000050}_{-0.000052}$	$85.530^{+0.017}_{-0.017}$		$4.805309^{+0.000004}_{-0.000005}$	$471.03^{+0.10}_{-0.07}$	
$a$ [ $R_\odot$ ]	$6.769^{+0.043}_{-0.034}$	$144.2^{+1.7}_{-0.9}$		$16.29^{+0.13}_{-0.13}$	$386.4^{+4.2}_{-3.4}$	
$e$	$0.0005^{+0.0005}_{-0.0003}$	$0.042^{+0.013}_{-0.013}$		$0.0050^{+0.0013}_{-0.0003}$	$0.4016^{+0.0039}_{-0.0038}$	
$\omega$ [deg]	$147^{+138}_{-97}$	$269.6^{+2.8}_{-3.1}$		$317^{+32}_{-35}$	$25.8^{+1.3}_{-1.5}$	
$i$ [deg]	$88.75^{+1.13}_{-1.13}$	$86.51^{+0.12}_{-0.13}$		$90.18^{+0.34}_{-0.29}$	$90.222^{+0.010}_{-0.009}$	
$\mathcal{T}_0^{\text{inf}}$ [BJD - 2400000] <sup>a</sup>	$58\,684.0427^{+0.0001}_{-0.0001}$	$59\,430.6949^{+0.0213}_{-0.0210}$		$58\,714.2412^{+0.0002}_{-0.0002}$	$58\,729.4535^{+0.0225}_{-0.0245}$	
$\tau$ [BJD - 2400000] <sup>b</sup>	$58\,683.56^{+0.20}_{-0.46}$	$59\,429.6^{+0.8}_{-0.7}$		$58\,710.46^{+0.38}_{-0.42}$	$58\,349.1^{+1.4}_{-1.6}$	
$\Omega$ [deg]	0.0	$-2.9^{+1.7}_{-3.1}$		0.0	$0.60^{+0.53}_{-0.48}$	
$i_{\text{mut}}$ [deg]		$3.5^{+3.3}_{-1.0}$		$0.69^{+0.49}_{-0.35}$		
mass ratio [ $q = m_{\text{sec}}/m_{\text{pri}}$ ]	$0.250^{+0.016}_{-0.015}$	$0.757^{+0.050}_{-0.019}$		$0.670^{+0.005}_{-0.005}$	$0.388^{+0.007}_{-0.006}$	
$K_{\text{pri}}$ [ $\text{km s}^{-1}$ ]	$59.4^{+3.3}_{-3.1}$	$36.7^{+1.7}_{-0.7}$		$68.84^{+0.44}_{-0.40}$	$12.67^{+0.23}_{-0.23}$	
$K_{\text{sec}}$ [ $\text{km s}^{-1}$ ]	$237.5^{+2.1}_{-2.3}$	$48.4^{+0.5}_{-0.8}$		$102.80^{+1.30}_{-1.06}$	$32.67^{+0.27}_{-0.24}$	
	Apsidal and nodal motion related parameters <sup>c</sup>					
$P_{\text{apse}}$ [year]	$0.80^{+0.02}_{-0.02}$	$889^{+33}_{-33}$		$417^{+6}_{-6}$	$2821^{+30}_{-29}$	
$P_{\text{apse}}^{\text{dyn}}$ [year]	$0.79^{+0.02}_{-0.02}$	$48.0^{+0.6}_{-1.6}$		$204^{+2}_{-3}$	$350^{+3}_{-3}$	
$P_{\text{node}}^{\text{dyn}}$ [year]		$50.7^{+1.8}_{-0.7}$			$399^{+5}_{-4}$	
$\Delta\omega_{3b}$ [arcsec/cycle]	$156^{+7}_{-3}$	$6321^{+224}_{-79}$		$79.4^{+1.0}_{-0.9}$	$4779^{+47}_{-45}$	
$\Delta\omega_{\text{GR}}$ [arcsec/cycle]	$3.81^{+0.05}_{-0.04}$	$0.315^{+0.008}_{-0.004}$		$1.26^{+0.04}_{-0.05}$	$0.088^{+0.003}_{-0.004}$	
$\Delta\omega_{\text{tide}}$ [arcsec/cycle]	$5014^{+123}_{-131}$	$1.7^{+0.1}_{-0.1}$		$2.93^{+0.15}_{-0.12}$	$0.00102^{+0.0005}_{-0.00004}$	
	stellar parameters					
	Aa	Ab	B	Aa	Ab	B
	Relative quantities and atmospheric properties					
fractional radius [ $R/a$ ]	$0.4239^{+0.0037}_{-0.0041}$	$0.2676^{+0.0046}_{-0.0045}$	$0.0573^{+0.0018}_{-0.0016}$	$0.0949^{+0.0007}_{-0.0006}$	$0.0549^{+0.0009}_{-0.0007}$	$0.00223^{+0.00008}_{-0.00006}$
temperature relative to ( $T_{\text{eff}}$ ) <sub>Aa</sub>	1	$0.548^{+0.016}_{-0.022}$	$0.559^{+0.024}_{-0.020}$	1	$0.803^{+0.006}_{-0.006}$	$0.786^{+0.008}_{-0.009}$
fractional flux [in <i>TESS</i> -band]	$0.3703^{+0.0122}_{-0.0125}$	$0.0372^{+0.0012}_{-0.0015}$	$0.5352^{+0.0478}_{-0.0265}$	$0.7644^{+0.0107}_{-0.0140}$	$0.1230^{+0.0016}_{-0.0016}$	$0.1039^{+0.0011}_{-0.0082}$
grav. dark. exponent [ $\beta$ ] <sup>d</sup>	$0.41^{+0.39}_{-0.25}$	$0.17^{+0.20}_{-0.13}$	...	...	...	...
albedo [ $A$ ] <sup>d</sup>	$0.97^{+0.05}_{-0.06}$	$0.76^{+0.05}_{-0.05}$	...	...	...	...
	Physical Quantities					
$m$ [ $M_\odot$ ]	$2.497^{+0.030}_{-0.025}$ <sup>d</sup>	$0.625^{+0.041}_{-0.038}$	$2.359^{+0.166}_{-0.061}$	$1.503^{+0.050}_{-0.038}$	$1.007^{+0.026}_{-0.021}$	$0.974^{+0.043}_{-0.034}$
$R$ [ $R_\odot$ ]	$2.871^{+0.031}_{-0.032}$	$1.812^{+0.039}_{-0.038}$	$8.242^{+0.313}_{-0.191}$	$1.547^{+0.023}_{-0.023}$	$0.894^{+0.023}_{-0.018}$	$0.861^{+0.039}_{-0.029}$
$T_{\text{eff}}$ [K]	$8977^{+380}_{-371}$	$4906^{+95}_{-108}$	$5019^{+40}_{-44}$ <sup>e</sup>	$6756^{+147}_{-157}$	$5421^{+81}_{-90}$	$5298^{+150}_{-119}$
$L_{\text{bol}}$ [ $L_\odot$ ]	$48.0^{+8.2}_{-6.9}$	$1.71^{+0.13}_{-0.14}$	$38.7^{+3.4}_{-2.6}$	$4.47^{+0.55}_{-0.49}$	$0.618^{+0.074}_{-0.059}$	$0.523^{+0.117}_{-0.077}$
$M_{\text{bol}}$	$0.54^{+0.17}_{-0.17}$	$4.16^{+0.09}_{-0.08}$	$0.77^{+0.14}_{-0.10}$	$3.14^{+0.13}_{-0.13}$	$5.29^{+0.11}_{-0.12}$	$5.47^{+0.17}_{-0.22}$
$M_V$	$0.60^{+0.12}_{-0.11}$	$4.50^{+0.15}_{-0.12}$	$1.06^{+0.08}_{-0.10}$	$3.09^{+0.13}_{-0.13}$	$5.42^{+0.14}_{-0.15}$	$5.65^{+0.22}_{-0.27}$
$\log g$ [dex]	$3.920^{+0.009}_{-0.008}$	$3.718^{+0.009}_{-0.009}$	$2.978^{+0.034}_{-0.025}$	$4.235^{+0.005}_{-0.004}$	$4.537^{+0.008}_{-0.011}$	$4.555^{+0.015}_{-0.020}$
	Global system parameters					
$\log(\text{age})$ [dex]					$8.77^{+0.12}_{-0.21}$	
$[M/H]$ [dex]					$0.36^{+0.04}_{-0.06}$	
$E(B - V)$ [mag]					$0.115^{+0.030}_{-0.034}$	
extra light $\ell_4$ [in <i>TESS</i> -band]		$0.054^{+0.025}_{-0.036}$			$0.007^{+0.009}_{-0.005}$	
$(M_V)_{\text{tot}}$		$0.03^{+0.10}_{-0.09}$			$2.88^{+0.13}_{-0.14}$	
distance [pc]		...			$623^{+19}_{-15}$	

Notes. <sup>a</sup>:  $\mathcal{T}_0^{\text{inf}}$  denotes the moment of an inferior conjunction of the secondary (Ab) and the tertiary (B) along their inner and outer orbits, respectively; <sup>b</sup>: time of periastron passage; <sup>c</sup>: for the meaning, significance and discussion of these parameters, see Sect. 3; <sup>d</sup>: gravitational darkening exponents ( $\beta$ ) and bolometric albedos ( $A$ ) were adjusted only for the inner pair of TIC 14839347 and, hence, these are given only in this case; <sup>e</sup>: taken from independent SED analysis with Gaussian priors.

which, together with a near Roche-lobe-filling secondary, make this inner binary appear to be a typical Algol-type system with a reversed mass ratio. The distant third star was found to be a little less massive than the current primary of the inner binary ( $m_B = 2.36_{-0.09}^{+0.17} M_\odot$ ).

This finding again emphasizes that, most likely, intensive mass exchange has occurred between the two inner binary stars in the near past of this triple system, as the tertiary component is evidently an evolved, red giant star ( $R_B = 8.2 \pm 0.3 R_\odot$ ), in contrast to the similarly massive, hot ( $T_{Aa} = 8975 \pm 380$  K) and much less evolved ( $R_{Aa} = 2.87 \pm 0.03 R_\odot$ ) primary component.

Here we emphasize again that, in the case of this particular system, we took into account the reflection/irradiation effect and, moreover, both the two gravity-darkening exponents and the bolometric albedos of the inner pair of stars were freely adjusted MCMC parameters. In the case of the hot and, hence, radiative primary star (component Aa) we obtained an albedo of  $A_{Aa} = 0.97 \pm 0.05$  which fits nicely with the theoretically expected value of  $A_{Aa}^{\text{theo}} = 1$ .<sup>4</sup> On the other hand, the bolometric albedo obtained for the convective secondary ( $A_{Ab} = 0.76 \pm 0.05$ ) significantly differs from the theoretically expected value of  $A_{Ab}^{\text{theo}} = 0.5$ . According to our knowledge, such a high albedo for a convective star is quite unusual, however, a deeper investigation of this question is beyond the scope of this paper.

Turning to the orbital properties of this triple system, we find that the inner orbit is circular, as is expected in the case of a nearly semi-detached system.<sup>5</sup> By contrast, the outer orbit displays some small, but significant, eccentricity ( $e_{\text{out}} = 0.04 \pm 0.01$ ). What makes this result, however, a bit less robust is that the secondary outer eclipses (in Sectors 14 and 55) are located exactly at phase 0.5. This is reflected by the fact that the outer argument of pericenter is  $\omega_{\text{out}} = 270^\circ \pm 3^\circ$  and, hence,  $e_{\text{out}} \cos \omega_{\text{out}} \approx 0$ . In turn, this would suggest that the outer orbit is seen exactly from the direction of its major axis. However, one should keep in mind that, in this particular case, the outer eccentricity is determined only via the weakly determined parameter  $e_{\text{out}} \sin \omega_{\text{out}}$ , which primarily manifests itself in the durations of the outer eclipses and has strong correlations with the outer inclination, the fractional radius of the tertiary, the node of the outer orbit relative to the inner one, and even some other parameters.<sup>6</sup>

As both the inner and outer orbits are fairly circular and almost coplanar ( $i_m = 3.5_{-1}^{+3}$ ), one cannot expect large perturbations and, hence, there are only small departures from Keplerian motions for the inner and outer orbits. This is true despite the fact that the nominal apsidal motion period of the inner orbit is shorter than a year ( $P_{\text{apse}} = 0.80 \pm 0.02$  yr). As one can see from the different kinds of apsidal advance rates  $\Delta\omega$ , in the case of the inner orbit the classic tidal ( $\Delta\omega_{\text{tide}}$ ) contribution is the dominant one—larger by one order of magnitude than that of the third-body driven apsidal motion. We emphasize again, however, that as the inner orbit is practically cir-

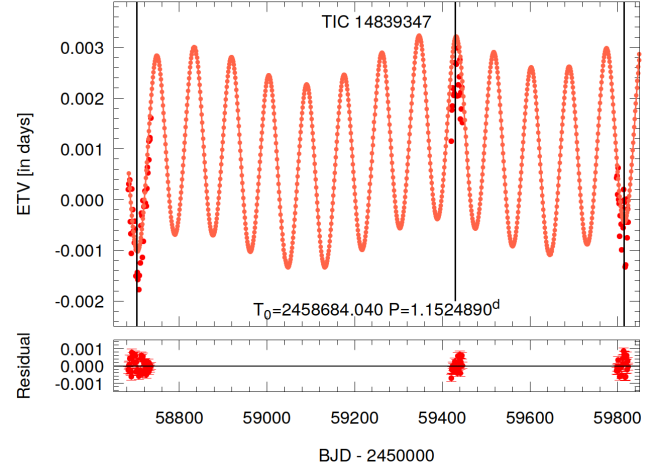


**Figure 4.** Photodynamical fit to the primary *TESS* ETV curve for TIC 14839347. The larger and darker red circles represent the observed primary times of EB eclipses, while the smaller, lighter symbols, connected with straight lines are taken from the photodynamical model ETV curve. The three thin vertical lines denote the locations of the three third-body outer eclipses. Residuals are also shown in the lower panel, where the uncertainty on each point is also noted.

cular, this very short apsidal motion is only virtual, stemming from the above mentioned slight imperfections in the use of osculating orbital elements in this particular case. On the other hand, for the small but clearly non-zero mutual inclination, one can expect a very low (few degrees) amplitude inclination variation with a period of  $P_{\text{node}}^{\text{dyn}} = 51 \pm 1$  yr, which might manifest itself in very small eclipse depth variations in the future.

Here we note also that the SED portion of the iterative solution for this system allowed for an age determination of the system of  $520 \pm 115$  Myr<sup>7</sup>, and an independent fit for the interstellar extinction of  $A_V = 2.2 \pm 0.16$ .

## 4.2 TIC 66893949

This system has the longest inner ( $P_{\text{in}} = 4.805$  d) and outer ( $P_{\text{out}} = 471.0$  d) periods. Because the *TESS* observations cover only 16-17% of the full outer orbit (see Fig. 5) it is quite surprising (and, of course, fortuitous) that both primary and secondary third-body eclipses were observed.

According to our photodynamical results, the system consists of three sun-like, main sequence stars ( $m_{Aa} = 1.51 \pm 0.04 M_\odot$ ,  $m_{Ab} = 1.01 \pm 0.02 M_\odot$ ,  $m_B = 0.97 \pm 0.04 M_\odot$ ). Note, amongst our four triple systems, this is the only one where the tertiary star was found to be the least massive.

In connection with the somewhat larger inner orbital separation, the inner binary pair has a small, but significant, eccentricity ( $e_{\text{in}} = 0.005 \pm 0.001$ ). The outer orbit also has the largest eccentricity in our sample with  $e_{\text{out}} = 0.402 \pm 0.004$ . Interestingly, despite the somewhat wide configuration, this triple was found to be quite flat ( $i_{\text{mut}} = 0.7 \pm 0.5$ ).

The dynamical timescales in this systems exceed several centuries

<sup>4</sup> In this regard, note that in their study Southworth et al. (2011) have obtained a clearly unphysical value of  $A > 2$  during the analysis of another semi-detached system with a hot primary. The authors explained this by the incompleteness of the physical model that they used – which happens to be very close to ours. Hence, this agreement we find with the theoretical value is far from trivial.

<sup>5</sup> Note that though our statistical results give an inner eccentricity of  $e_{\text{in}} = 0.0005 \pm 0.0004$ , this is only for the instantaneous osculating orbital elements, which, in general, cannot result in exactly zero eccentricity in a perturbed Keplerian problem. This question was discussed in detail e.g. in Kiseleva et al. (1998); Borkovits et al. (2002).

<sup>6</sup> As one can readily see in Fig. 4, the ETV curve is currently so poorly covered that it does not carry any information about the eccentricity of the outer orbit.

<sup>7</sup> Here we assumed that even though the inner binary stars may have previously exchanged mass, the tertiary star has not been affected and is evolving normally as a single star.

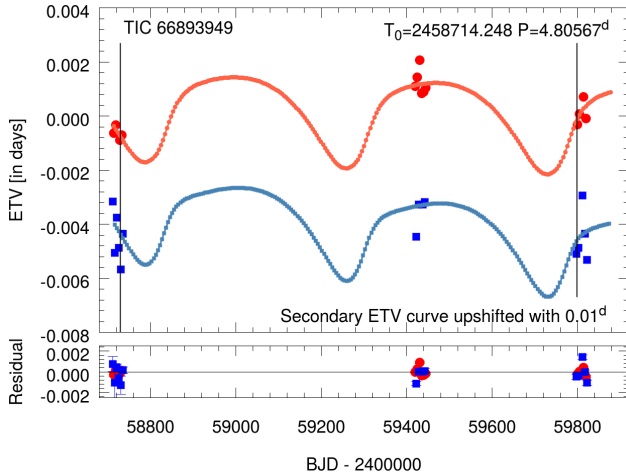


**Figure 5.** Photodynamical fit to the *TESS* ETV curves for TIC 6893949. The larger and darker red circles and blue squares represent the observed primary and secondary times of EB eclipses, while the smaller, lighter symbols, connected with straight lines are taken from the photodynamical model ETV curve. The two thin vertical lines denote the locations of the two third-body outer eclipses. Residuals are also shown in the lower panel, where the uncertainty on each point is also noted.

for both the inner and outer subsystems. Moreover, as one can see from the separate apsidal advance rates, both the classic tidal and the relativistic contributions to the apsidal motions are negligible relative to the dynamical (forced by third-body perturbations) apsidal motions of the inner and outer orbits.

Finally, we note that our analysis resulted in a slightly larger distance than that of [Bailer-Jones et al. \(2021\)](#), i.e.,  $d_{\text{phot}} = 625 \pm 17$  pc, vs.  $d_{\text{EDR3}} = 587 \pm 9$  pc, a  $2 - \sigma$  discrepancy.

### 4.3 TIC 88206187

Despite the fact that this triple was observed only in two *TESS* sectors, we were able to obtain the most robust solution for this system among those studied in this work. The reason is that, fortunately, *TESS* observed both primary and secondary third-body eclipses and, moreover, both the inner and outer eclipses are total (i.e., having flat-bottom mid-eclipse sections) which strongly constrain the surface brightness ratios of the constituent stars. Moreover, the combination of the *TESS* observations with the archive ground-base data (see Sect. 2.2) we were able to determine the outer period with considerable accuracy ( $P_{\text{out}} = 52.84 \pm 0.01$  days) which was found to be in reasonable agreement with that of the somewhat less accurate *Gaia* SB1 solution ( $P_{\text{out}} = 53.03 \pm 0.06$  days; Table 4). This makes this triple the most compact in our sample.

Already, a very first inspection of the 2-day-long primary third-body eclipse around BJD 2 458 829 (at the middle of Sector 19, see lower left panel of Fig. 1) reveals that the tertiary is likely the largest component and, most probably, is a red giant star.<sup>8</sup> The unequal primary and secondary third-body eclipse depths, with the flat bottom of the much deeper (primary) third-body eclipse, indicate that the

members of the inner EB are much smaller, but substantially hotter, than the tertiary star. From this, one can directly infer that the tertiary component should be the most massive amongst the three stars, being the most evolved (assuming, of course, coeval evolution for the three objects). Finally, the fact that, in the case of the primary third-body eclipse (at Sector 19) the tertiary component passes its inferior conjunction point, reveals the outer orbital phase at that (or any other) moment uniquely, despite the absence of any informative ETV data (see Fig. 6).

The photodynamical solution then confirmed all these preliminary assessments, as it was found that the tertiary star was actually a moderately massive ( $m_B = 2.6 \pm 0.1 M_{\odot}$ ) red giant star with the basic parameters of  $R_B = 11.7 \pm 0.3 R_{\odot}$  and  $T_B = 4950 \pm 70$  K. The members of the inner binary pair, however, were found to be A and F-type, but still MS stars, with parameters of  $m_{Aa,Ab} = 2.05 \pm 0.05 M_{\odot}$ ,  $1.35 \pm 0.03 M_{\odot}$ ;  $R_{Aa,Ab} = 2.25 \pm 0.05 R_{\odot}$ ,  $1.35 \pm 0.03 R_{\odot}$ ;  $T_{Aa,Ab} = 8360^{+270}_{-160}$  K,  $6590^{+170}_{-70}$  K for the primary and secondary binary components, respectively.

The future evolution of this triple seems to be quite interesting. Due to the compactness of both the inner and outer subsystems, we may expect that both the currently more massive red giant tertiary and the TAMS-aged primary of the inner binary will fill out their respective Roche-lobes. The current size of the tertiary and its Roche lobe radius are  $11.7 R_{\odot}$  and  $38.3 R_{\odot}$ , respectively. The same quantities for the primary EB star, Aa, are  $2.25 R_{\odot}$  and  $2.94 R_{\odot}$ , respectively. Thus, star Aa needs to increase its radius only by  $\approx 30\%$  in order to overflow its Roche lobe, whereas the tertiary would need to triple its current radius to overflow its Roche lobe. Nonetheless, according to MIST stellar evolution tracks ([Dotter 2016](#); [Choi et al. 2016](#)) it will take star Aa some 260 Myr to reach a state where it overflows its Roche lobe with respect to star Ab. By contrast, the more massive and currently more evolved tertiary star will evolve much more rapidly and will reach the tip of the red giant branch (RGB) in a few Myr. At that time, its radius will not quite be sufficiently large to fill its Roche lobe. However, in less than 180 Myr after that, it will ascend the asymptotic giant branch (AGB) and overflow its Roche lobe for certain.

The detailed evolution of this system, after mass transfer from the giant tertiary to the inner binary commences, is beyond the scope of this paper. However, we can speculate that since the tertiary will be a convective giant at that time, and the outer mass ratio ( $m_B/(m_{Aa} + m_{Ab})$ ) is 0.76, the mass transfer could be dynamically stable. But, formally, for a completely convective donor star, this ratio should be  $\lesssim 2/3$ .

Apart from its future evolution with mass transfer, this triple may harbour other interesting effects in its present configuration as well. Recently [Gao et al. \(2023\)](#) called attention to the fact that such compact triple stars, where the tertiaries are red giants, may produce remarkable tidal effects whereby tidal dissipation could lead to observable orbital shrinkage within some decades-long timescales. In this regard, we note that amongst all the known analysed compact triple star systems, TIC 88206187 is only the third case in which the fractional radius of the distant tertiary exceeds 0.1 ( $r_B = R_B/a_{\text{out}} = 0.109 \pm 0.002$ )<sup>9</sup>, and thus, tertiary tides might currently be effective, at least marginally. In this regard, also note that, despite the relatively more significant apsidal advance rate of the outer orbit due to tidal forcing ( $\Delta\omega_{\text{tide}} = 9'' \pm 1''/\text{cycle}$ ), it is clearly negligible relative to

<sup>8</sup> Note that amongst other *TESS*-discovered triply eclipsing triples, analyzed in former papers, it is TIC 54060695 whose LC (more strictly speaking, the third-body eclipses) most closely resembles that of the current triple system (see the middle left panel of Fig. 1 of [Rappaport et al. 2022](#)).

<sup>9</sup> The other two systems are TIC 242132789 ([Rappaport et al. 2022](#)) and HD 181068 ([Borkovits et al. 2013](#); [Fuller et al. 2013](#)) with  $r_B = 0.151$  and  $0.138$ , respectively.



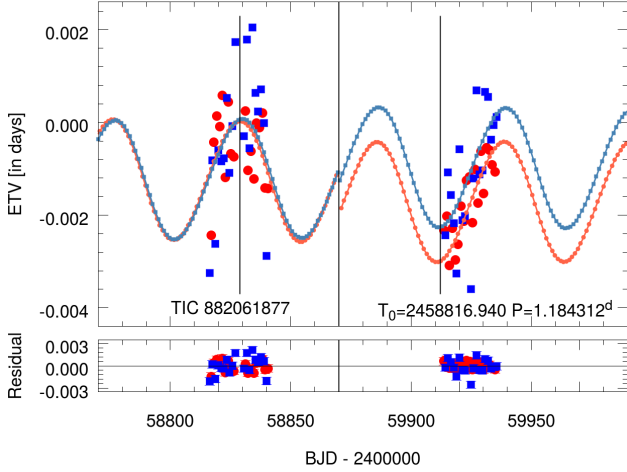


**Figure 6.** Photodynamical fit to the *TESS* ETV curves for TIC 882061877.

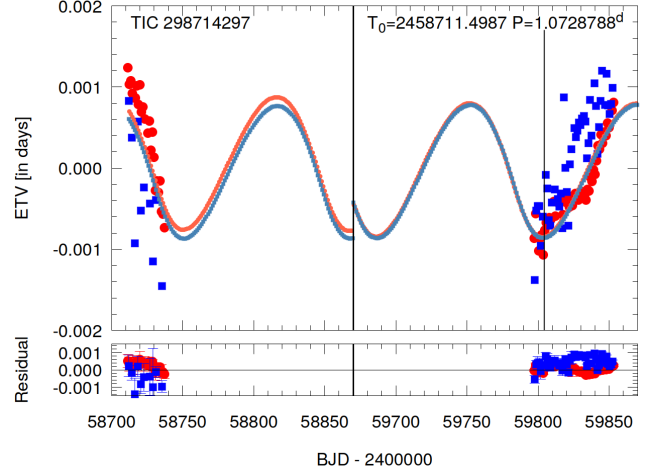


**Figure 7.** Photodynamical fit to the *TESS* ETV curves for TIC 298714297.

the third-body effects ( $\Delta\omega_{\text{tide}} = 11400'' \pm 100''/\text{cycle}$ ) and does not alter the timescale of the apsidal precession ( $P_{\text{apse}} = 185 \pm 1$  yr).

Finally, we note that the photometric distance inferred from our analysis is  $d_{\text{phot}} = 2580 \pm 60$  pc, which is in quite a good agreement with the *Gaia*-parallax inferred distance of  $d_{\text{EDR3}} = 2490 \pm 90$  pc (Bailer-Jones et al. 2021).

#### 4.4 TIC 298714297

In contrast to the other systems in this study, TIC 298714297 is found to be a triplet of three low-mass cool red (K and M-type) dwarfs. Besides the three dips of a complex third-body eclipse, the other remarkable feature of the LC is the likely rotational distortions, caused by stellar spots, which are most pronounced in the Sector 55, 56 LCs. Moreover, the system shows three sudden, short  $\sim 3 - 4\%$  brightenings which we attribute to stellar flares.

All these features suggest strong chromospheric/photospheric stellar activity on at least one of the stellar components. In the case of the rotational modulation, since the observed period is equal, or very close to, the period of the inner EB, it seems quite likely that its origin is component Aa (which is the most massive and brightest amongst the three stars). In the case of the three stellar flare events, their origin, strictly speaking, is less certain. But, considering the other signals of strong magnetic activity are likely from star Aa, we may tentatively assume that the flare events are also hosted by this star. It is noteworthy, however, that the two larger flares were observed during Sector 15, when the rotational modulation (i.e., due to the spottedness) was much less pronounced.

Regarding the astrophysical parameters, this triple was found to be not only the least massive ( $m_{\text{Aa}} = 0.83 \pm 0.03 M_{\odot}$ ,  $m_{\text{Ab}} = 0.50 \pm 0.02 M_{\odot}$ ,  $m_{\text{B}} = 0.68 \pm 0.02 M_{\odot}$ ) of our set, but also the most aged ( $\tau \sim 10$  Gyr). Note, however, that some caution is necessary, as our model solution resulted in a reddening of  $E(B-V) = 0.3 \pm 0.08$  which looks quite unrealistic for such a close object ( $d_{\text{phot}} = 138 \pm 4$  pc vs.  $d_{\text{EDR3}} = 111.9 \pm 0.7$  pc Bailer-Jones et al. 2021).

The inner orbit was found to be practically circular ( $e_{\text{in}} = 0.002^{+0.007}_{-0.001}$ ) which is naturally expected for such an old and close binary, while the outer orbit was found to be moderately eccentric ( $e_{\text{out}} = 0.24 \pm 0.03$ ). In this regard, we note that the secondary's ETV curve in the inner EB is offset a little from the primary's one (Fig. 7). However, in our interpretation, in this case such an offset is

not due a slight orbital eccentricity, but rather is caused by the LC variations due to the starspots on at least one of the stars. Such shifts in the ETVs were found by Tran et al. (2013).

Finally, note also that besides TIC 14839347, this is the other system in our sample where the apsidal motion of the inner orbit is dominated by the tidal forces instead of third-body perturbations ( $\Delta\omega_{\text{tide}} = 105'' \pm 10''/\text{cycle}$  vs.  $\Delta\omega_{\text{3b}} = 63'' \pm 2''/\text{cycle}$ ). But, again, due to the very low inner eccentricity one cannot expect strong, non-Keplerian variations during the apsidal motion cycle of  $P_{\text{apse}} = 28 \pm 2$  yr.

## 5 COMPARING ORBITAL PARAMETERS WITH GAIA

In general, we find substantial agreement between the *Gaia* and photodynamical results for the four systems studied in this work. As far as we can judge, however, our results are generally the more accurate ones. Having said this, however, there are a number of caveats to discuss. First, we note that a comparison of the orbital elements from the *Gaia* NSS solution and those from the LIGHTCURVEFACTORY photodynamical models is limited due to the differences in their methodologies. The *Gaia* NSS solutions adopt a Keplerian two-body orbit model, whereas the calculated orbital elements from LIGHTCURVEFACTORY represent instantaneous osculating elements. Consequently, the orbital elements obtained from these two approaches are not exactly comparable. However, for the four sources studied in this work, the perturbations to the motions along the outer orbits are negligible on the timescale of the *Gaia* observation interval, and therefore they do not result in significant discrepancies on this account. For example, the apsidal motion timescales of the outer orbits in all our four triples range from 185 yr to 2820 yr. Hence, the orientations of the astronomical orbits measured by *Gaia* will vary by only a negligible amount during the full operation of the space telescope. Moreover, due to the flatness of the four systems, no significant variations in the outer inclinations will occur. One can therefore expect that the orbits will remain (almost) pure Keplerian over the entire life cycle of *Gaia*.

Another issue is that in the *Gaia* DR3 catalogue, the NSS solutions are limited to spatially unresolved stellar systems, primarily due to the specific data processing constraints employed by the *Gaia* team. In the case of astrometric solutions (i.e., for TIC 298714297 and TIC 66893949) *Gaia* measures only the orbit of the photocenter of

**Table 3.** Orbital and astrophysical parameters of TICs 88206187 and 298714297 from the joint photodynamical *TESS*, ETV, SED and PARSEC isochrone solution. Note that the orbital parameters are instantaneous, osculating orbital elements and are given for epoch  $t_0$  (first row).

	TIC 88206187			TIC 298714297		
	orbital elements					
	subsystem			subsystem		
	Aa–Ab	A–B		Aa–Ab	A–B	
$t_0$ [BJD - 2400000]	58 816.0			58 711.0		
$P$ [days]	$1.184592^{+0.000055}_{-0.000063}$	$52.922^{+0.041}_{-0.039}$		$1.072891^{+0.000010}_{-0.000019}$	$117.24^{+0.36}_{-0.31}$	
$a$ [ $R_\odot$ ]	$7.085^{+0.053}_{-0.061}$	$107.7^{+1.1}_{-1.0}$		$4.863^{+0.050}_{-0.077}$	$127.5^{+1.3}_{-1.8}$	
$e$	$0.0012^{+0.0005}_{-0.0005}$	$0.026^{+0.017}_{-0.013}$		$0.0019^{+0.0072}_{-0.0009}$	$0.241^{+0.029}_{-0.028}$	
$\omega$ [deg]	$75^{+21}_{-27}$	$147^{+100}_{-27}$		$84^{+71}_{-10}$	$28^{+8}_{-6}$	
$i$ [deg]	$89.86^{+2.36}_{-1.98}$	$89.54^{+0.73}_{-0.75}$		$89.00^{+0.93}_{-0.79}$	$89.86^{+0.10}_{-0.05}$	
$\mathcal{T}_0^{\text{inf/sup}}$ [BJD - 2400000]	$58\,816.9391^{+0.0002}_{-0.0002}$	$58\,828.8819^{+0.0081}_{-0.0081}$		$58\,711.4972^{+0.0002}_{-0.0001}$	$59\,804.6649^{+0.0396*}_{-0.0385}$	
$\tau$ [BJD - 2400000]	$58\,816.292^{+0.067}_{-0.094}$	$58\,800.2^{+15.1}_{-13.8}$		$58\,710.942^{+0.213}_{-0.029}$	$59\,791.8^{+2.0}_{-1.6}$	
$\Omega$ [deg]	0.0	$-1.17^{+3.01}_{-2.18}$		0.0	$4.23^{+4.33}_{-4.13}$	
$i_{\text{mut}}$ [deg]		$2.90^{+1.63}_{-1.37}$			$4.41^{+4.18}_{-2.70}$	
mass ratio [ $q = m_{\text{sec}}/m_{\text{pri}}$ ]	$0.661^{+0.009}_{-0.009}$	$0.765^{+0.010}_{-0.017}$		$0.617^{+0.013}_{-0.016}$	$0.512^{+0.007}_{-0.009}$	
$K_{\text{pri}}$ [ $\text{km s}^{-1}$ ]	$120.36^{+1.02}_{-0.92}$	$44.48^{+0.97}_{-0.71}$		$87.26^{+2.14}_{-2.02}$	$19.12^{+0.34}_{-0.27}$	
$K_{\text{sec}}$ [ $\text{km s}^{-1}$ ]	$182.26^{+1.83}_{-2.40}$	$58.47^{+0.71}_{-0.37}$		$141.79^{+1.14}_{-1.94}$	$37.48^{+0.57}_{-0.60}$	
Apsidal and nodal motion related parameters						
$P_{\text{apse}}$ [year]	$7.3^{+0.2}_{-0.3}$	$185^{+1}_{-1}$		$27.8^{+1.9}_{-2.2}$	$1124^{+30}_{-34}$	
$P_{\text{apse}}^{\text{dyn}}$ [year]	$5.2^{+0.1}_{-0.2}$	$16.41^{+0.16}_{-0.09}$		$22.4^{+1.2}_{-1.5}$	$104^{+2}_{-3}$	
$P_{\text{node}}^{\text{dyn}}$ [year]		$18.0^{+0.1}_{-0.2}$			$114^{+3}_{-2}$	
$\Delta\omega_{3b}$ [arcsec/cycle]	$443^{+4}_{-5}$	$11433^{+62}_{-113}$		$63.4^{+1.6}_{-1.5}$	$4013^{+105}_{-85}$	
$\Delta\omega_{\text{GR}}$ [arcsec/cycle]	$3.96^{+0.06}_{-0.07}$	$0.459^{+0.10}_{-0.008}$		$2.28^{+0.05}_{-0.07}$	$0.014^{+0.004}_{-0.004}$	
$\Delta\omega_{\text{tide}}$ [arcsec/cycle]	$362^{+24}_{-17}$	$9.0^{+0.9}_{-0.8}$		$104^{+12}_{-9}$	$0.025^{+0.002}_{-0.002}$	
stellar parameters						
	Aa	Ab	B	Aa	Ab	B
Relative quantities						
fractional radius [ $R/a$ ]	$0.3185^{+0.0047}_{-0.0039}$	$0.1905^{+0.0030}_{-0.0028}$	$0.1086^{+0.0021}_{-0.0020}$	$0.1728^{+0.0026}_{-0.0025}$	$0.1042^{+0.0050}_{-0.0043}$	$0.0053^{+0.0001}_{-0.0001}$
temperature relative to ( $T_{\text{eff}}^{\text{Aa}}$ )	1	$0.789^{+0.010}_{-0.010}$	$0.592^{+0.010}_{-0.012}$	1	$0.678^{+0.006}_{-0.007}$	$0.840^{+0.015}_{-0.013}$
fractional flux [in <i>TESS</i> -band]	$0.1600^{+0.0027}_{-0.0026}$	$0.0294^{+0.0011}_{-0.0011}$	$0.800^{+0.008}_{-0.015}$	$0.6794^{+0.0386}_{-0.0335}$	$0.0532^{+0.0029}_{-0.0026}$	$0.2062^{+0.0191}_{-0.0217}$
Physical Quantities						
$m$ [ $M_\odot$ ]	$2.047^{+0.051}_{-0.061}$	$1.349^{+0.031}_{-0.026}$	$2.589^{+0.107}_{-0.090}$	$0.827^{+0.024}_{-0.036}$	$0.508^{+0.024}_{-0.025}$	$0.678^{+0.026}_{-0.022}$
$R$ [ $R_\odot$ ]	$2.253^{+0.048}_{-0.034}$	$1.349^{+0.030}_{-0.028}$	$11.71^{+0.28}_{-0.30}$	$0.839^{+0.021}_{-0.023}$	$0.506^{+0.030}_{-0.028}$	$0.669^{+0.022}_{-0.018}$
$T_{\text{eff}}$ [K]	$8358^{+279}_{-154}$	$6587^{+169}_{-72}$	$4947^{+70}_{-59}$	$5332^{+106}_{-198}$	$3620^{+55}_{-121}$	$4463^{+133}_{-137}$
$L_{\text{bol}}$ [ $L_\odot$ ]	$22.6^{+2.5}_{-2.0}$	$3.13^{+0.28}_{-0.23}$	$74.0^{+4.6}_{-4.3}$	$0.504^{+0.037}_{-0.040}$	$0.039^{+0.004}_{-0.004}$	$0.159^{+0.019}_{-0.016}$
$M_{\text{bol}}$	$1.39^{+0.10}_{-0.12}$	$3.53^{+0.08}_{-0.09}$	$0.10^{+0.07}_{-0.07}$	$5.51^{+0.09}_{-0.08}$	$8.30^{+0.11}_{-0.11}$	$6.77^{+0.11}_{-0.12}$
$M_V$	$1.35^{+0.09}_{-0.08}$	$3.50^{+0.09}_{-0.09}$	$0.38^{+0.07}_{-0.09}$	$5.67^{+0.15}_{-0.10}$	$9.82^{+0.33}_{-0.19}$	$7.41^{+0.23}_{-0.23}$
$\log g$ [dex]	$4.040^{+0.010}_{-0.011}$	$4.307^{+0.010}_{-0.010}$	$2.713^{+0.016}_{-0.016}$	$4.505^{+0.010}_{-0.012}$	$4.733^{+0.027}_{-0.030}$	$4.617^{+0.009}_{-0.012}$
Global system parameters						
$\log(\text{age})$ [dex]		$8.81^{+0.04}_{-0.05}$			$10.02^{+0.04}_{-0.04}$	
$[M/H]$ [dex]		$0.17^{+0.07}_{-0.16}$			$-0.01^{+0.23}_{-0.18}$	
$E(B - V)$ [mag]		$0.28^{+0.04}_{-0.02}$			$0.30^{+0.05}_{-0.09}$	
extra light $\ell_4$ [in <i>TESS</i> -band]		$0.010^{+0.015}_{-0.008}$			$0.05^{+0.05}_{-0.04}$	
$(M_V)_{\text{tot}}$		$-0.03^{+0.07}_{-0.08}$			$5.45^{+0.17}_{-0.12}$	
distance [pc]		$2584^{+53}_{-68}$			$138^{+4}_{-4}$	

Notes.  $\mathcal{T}_0^{\text{inf/sup}}$  denotes the moment of an inferior or superior conjunction of the secondary (Ab) and the tertiary (B) along their inner and outer orbits, respectively. Superior conjunctions are noted with \*.

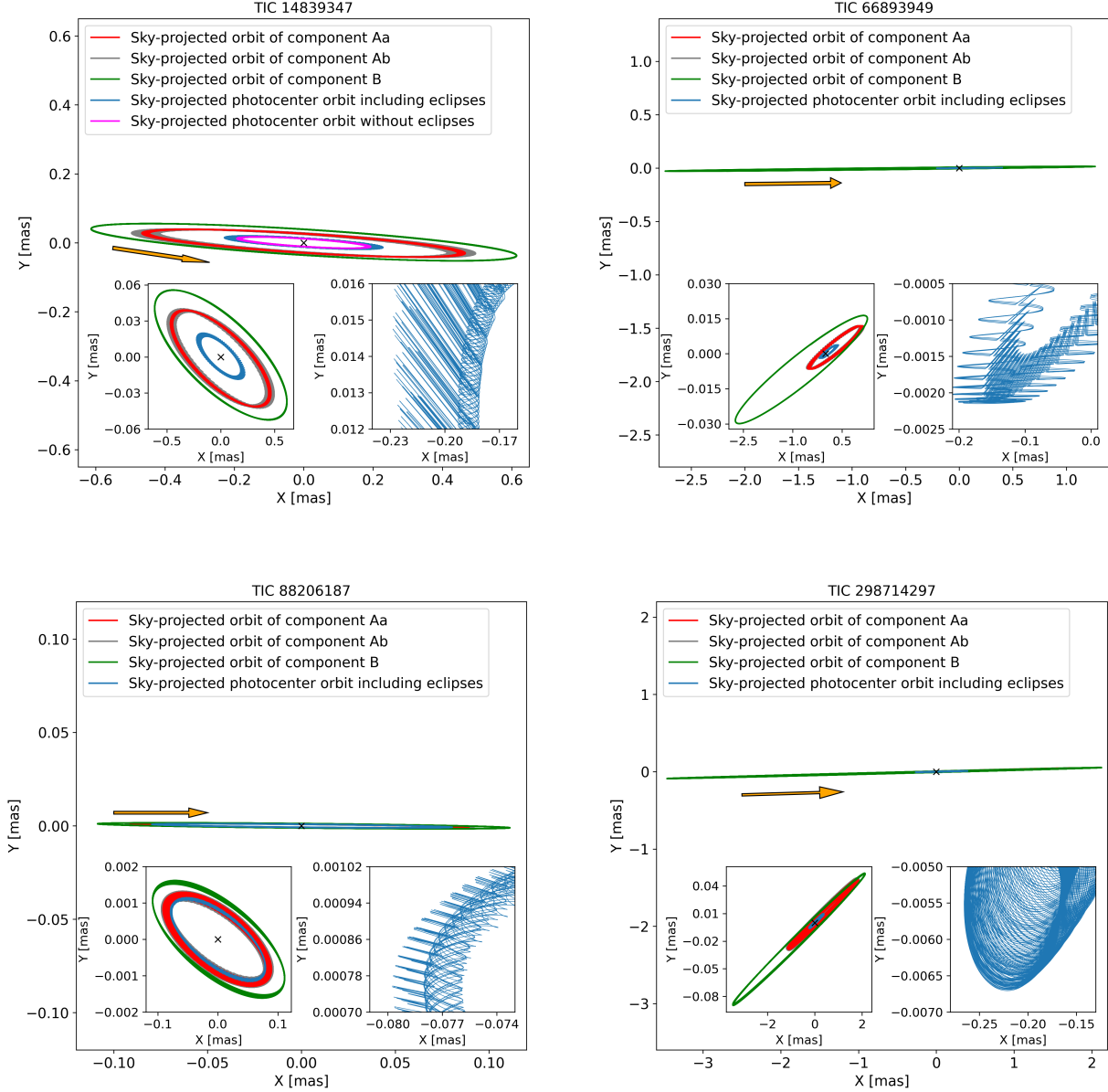


**Figure 8.** Astrometric orbits for each stellar component in all four investigated triple systems, together with our *calculated* photocenter orbits, the latter of which are only measurable by *Gaia*. The sky positions and therefore, the astrometric orbits of all the components were taken directly from the numerical integrator of LIGHTCURVEFACTORY. These were then converted into milliarcseconds from their original physical dimensions according to the photometric distances obtained from the photodynamical solutions. The positions of the photocenters were calculated from the flux-weighted averages of the individual stellar positions, according to Eqs. (C1–C2) of Rappaport et al. (2022). For each plot there are also two smaller, insert figures. In the left inserts we show again the astrometric orbits, but with unequally scaled  $x$  and  $y$  axes for a better view of the nearly edge-on and, consequently, near straight line-like sky-projected orbits. In the right inserts we display zoomed short sections of the photocenter orbits, where the rapid flux variations caused by the inner eclipses are also taken into account. As one can see, these eclipses produce sudden, quasi discontinuous shifts in the photocenter, which may result in higher scatter and, hence, increased uncertainties in the astrometric orbital elements.

the three stars, and not of any of the individual constituent members within the triple system (Marcussen & Albrecht 2023; Eq. C2 of Rappaport et al. 2022). This fact, however, may produce some departures from pure Keplerian astrometric orbits, as during the relatively deep primary eclipses of the four inner pairs, one may expect some quasi-

discontinuous shifts in the positions of the photocenter.<sup>10</sup> In order to illustrate these effects, we plot the theoretically expected photocenter

<sup>10</sup> Naturally, the same holds for the astrometric measurements during third-body eclipses, where these discontinuities might be even much larger. However, due the rarity of the extra eclipse events, observations during these events are less likely.

orbits (together with the above mentioned potential discontinuities in the small, inserted plots) for all four investigated systems in Fig. 8. Keeping in mind all of the above discussion, we conclude that the only direct comparisons that can be made for these systems with the photodynamical results are the period, the eccentricity, and the inclination of the outer orbit. In the cases involving the *Gaia* spectroscopic orbits (i.e., TIC 88206187 and TIC 14839347), *Gaia* primarily observes the spectral lines of the more luminous tertiary component. Thus we can also compare the *Gaia* RV semi-amplitude ( $K_1$ ) of the outer tertiary with the value from the photodynamical fit.

A third issue is that generally the argument of periastron of the outer orbit from the *Gaia* measurements and those of the photodynamical results typically differ by  $180^\circ$ . This is due to the fact that *Gaia* is generally tracking the brighter tertiary, while the photodynamical analysis utilizes the ETV points from the inner binary.

Finally, with these caveats in mind, we compare the *Gaia* and photodynamical analysis in Table 4. We find generally good agreement for the outer orbital period and its inclination angle. However, in the case of the outer eccentricity, the differences are mostly larger, but in the case of TIC 66893949, for example, the two values are in good agreement.

## 6 SUMMARY AND CONCLUSIONS

The most common method for discovering triply eclipsing triple star systems involves searching for evidence of a third-body eclipse in the extended time series of EB systems. These utilize the extensive time series datasets obtained from the *TESS* or *Kepler* photometric sky survey telescopes. The searches are usually done by eye or with the assistance of machine learning tools (see, e.g., Rappaport et al. 2022, 2023). It goes without saying that the longer the duration of a data set the greater the likelihood of identifying eclipses involving third bodies within a given system.

In our previous paper (Czavalinga et al. 2023), we reported the discovery of four triply eclipsing triple systems using an alternative method that utilizes the *Gaia* DR3 data set. In that study, we cross-matched a catalog of approximately 1 million binaries with *Gaia* stars that had longer-period NSS orbital solutions. Of the  $\sim 400$  triple systems found in that study, four of them turned out to also be triply eclipsing, as discovered through the use of *TESS* data. Though the fractional yield was small (1%), this still demonstrated the effectiveness of alternative methods in the search for triply eclipsing triples.

In this work, we studied these four triply eclipsing systems in detail using precision ETV curves and photometry from *TESS* data, archival photometry from ASAS-SN and ATLAS, and archival SED curves. These input data sets undergo a comprehensive analysis via a spectro-photodynamics code (LIGHTCURVEFACTORY) to yield both the stellar and orbital parameters of the systems. In general, the four new compact triples are not dissimilar to ones our group has been studying over the past number of years.

TIC 66893949 consists of stars with masses similar to our Sun. This system has the longest outer period among the triples investigated in our sample, and it has the most eccentric outer orbit  $e_{\text{out}} \approx 0.4$ . Even though it has a wide configuration, the mutual inclination angle is fairly low at  $i_{\text{mut}} = 0.6 \pm 0.5$  degrees.

TIC 88206187 has the shortest outer period in our sample  $P_{\text{out}} = 52.92 \pm 0.04$  days, and contains a tertiary red giant star with radius of  $11.7 \pm 0.3R_{\odot}$ . This represents only the third system discovered thus far in which the fractional radius (i.e.,  $R/a$ ) of the distant tertiary component exceeds 0.1, suggesting the presence of ongoing tidal effects. Our photodynamical model benefitted from the ATLAS

and ASAS-SN LCs which show both the outer primary and secondary eclipses, and therefore provide a precise period and a value for  $e_{\text{out}} \cos \omega_{\text{out}}$ . From the MIST stellar evolution tracks, we find that it is likely that the outer tertiary will be the first star in the system to fill its Roche lobe when it becomes an AGB star and transfer mass to the inner binary pair.

TIC 298714297 is one of the closest triply eclipsing triple systems ever found with a distance of  $138 \pm 4$  pc. It contains low-mass stars that exhibit pronounced spot activity in one of the components of the inner binary, with several flares identified. The most probable host of these flares is star Aa with the largest luminosity in the system.

We encountered some difficulties with modelling TIC 14839347. The low mass secondary component of the inner pair was found to be strongly non-spherical, filling or nearly filling its Roche lobe, which hints at a previous episode of mass transfer. Consequently, the use of the PARSEC single-star evolutionary tracks within the LIGHTCURVEFACTORY analysis could not be used. However, we were able to use a separate SED fitting code (Rappaport et al. 2022) that does not assume any physical relation between the radius and  $T_{\text{eff}}$  of either binary star, and which can estimate the stellar properties of all three stars. That code, in turn, used estimates of a number of dimensionless ratios such as of the radii and  $T_{\text{eff}}$  which we could get from LIGHTCURVEFACTORY. Since neither code could proceed without results from the other, we ran them iteratively until a satisfactory solution was achieved. From this analysis we find that the inner binary has a mass ratio of  $0.25 \pm 0.04$  and, as mentioned above, the secondary is nearly filling its Roche lobe. Therefore the inner binary appears as an Algol system with an inverted mass ratio. The outer stellar component is an evolved red giant star, while the primary star of the inner binary appears to be less evolved than the tertiary though these two stars are similar in mass. This feature may also be explained by the fact that a mass exchange event has occurred between the inner binary stars in the near past.

The use of *Gaia* DR3 NSS solutions have demonstrated the value of exploring triple systems using alternative methodologies. The upcoming release of *Gaia* DR4 will provide even more extensive data, making it extremely worthwhile to search for signs of triples within these datasets and subsequently perform photodynamical analyses on them. Such a greatly enhanced statistical sample of compact triples should yield a more comprehensive understanding of these important, intriguing, and fun systems.

## ACKNOWLEDGEMENTS

A. P. acknowledges the financial support of the Hungarian National Research, Development and Innovation Office – NKFIH Grant K-138962.

This paper includes data collected by the *TESS* mission. Funding for the *TESS* mission is provided by the NASA Science Mission directorate. Some of the data presented in this paper were obtained from the Mikulski Archive for Space Telescopes (MAST). STScI is operated by the Association of Universities for Research in Astronomy, Inc., under NASA contract NAS5-26555. Support for MAST for non-HST data is provided by the NASA Office of Space Science via grant NNX09AF08G and by other grants and contracts.

This work has made use of data from the European Space Agency (ESA) mission *Gaia*<sup>11</sup>, processed by the *Gaia* Data Processing and Analysis Consortium (DPAC)<sup>12</sup>. Funding for the DPAC has been

<sup>11</sup> <https://www.cosmos.esa.int/gaia>

<sup>12</sup> <https://www.cosmos.esa.int/web/gaia/dpac/consortium>



**Table 4.** Comparison of orbital parameters of the outer orbit between LIGHTCURVEFACTORY and *Gaia* DR3 NSS solution. For each object, the upper values belong to the LIGHTCURVEFACTORY, while the lower values correspond to the *Gaia* DR3 NSS solution.

Name	NSS model	P[days]	e	$\omega$ [deg]	a[R <sub>⊙</sub> ]	i[deg]	K <sub>sec</sub> [km/s]
TIC 14839347	SB1	85.524 <sup>+0.0017</sup> 85.315 ± 0.2458 <sub>-0.0015</sub>	0.047 <sup>+0.011</sup> 0.022 ± 0.057 <sub>-0.013</sub>	269.9 <sup>+2.8</sup> 44.0 ± 156.3 <sub>-3.3</sub>	-	-	46.4 <sup>+0.5</sup> 50.3 ± 2.6 <sub>-0.7</sub>
TIC 66893949	Orbital	471.03 <sup>+0.10</sup> 470.72 ± 3.37 <sub>-0.07</sub>	0.4016 <sup>+0.0039</sup> 0.404 ± 0.065 <sub>-0.0038</sub>	25.8 <sup>+1.3</sup> 237.011 ± 8.744 <sub>-1.5</sub>	386.4 <sup>+4.2</sup> 72.09 ± 2.48 <sub>-3.4</sub>	90.222 <sup>+0.010</sup> 91.39 ± 1.37 <sub>-0.009</sub>	-
TIC 88206187	SB1	52.922 <sup>+0.041</sup> 53.035 ± 0.058 <sub>-0.039</sub>	0.026 <sup>+0.017</sup> 0.100 ± 0.044 <sub>-0.013</sub>	147 <sup>+100</sup> 212 ± 9 <sub>-99</sub>	-	-	58.47 <sup>+0.41</sup> 65.23 ± 3.54 <sub>-0.37</sub>
TIC 298714297	Orbital	117.25 <sup>+0.36</sup> 118.60 ± 0.28 <sub>-0.31</sub>	0.242 <sup>+0.029</sup> 0.185 ± 0.065 <sub>-0.029</sub>	28 <sup>+8</sup> 161 ± 20 <sub>-7</sub>	127.3 <sup>+1.3</sup> 16.37 ± 0.50 <sub>-1.8</sub>	89.86 <sup>+0.09</sup> 89.53 ± 2.21 <sub>-0.05</sub>	-

provided by national institutions, in particular the institutions participating in the *Gaia* Multilateral Agreement.

We have made use of the All-Sky Automated Survey for Supernovae archival photometric data. See (Shappee et al. 2014) and (Kochanek et al. 2017) for details of the ASAS-SN survey. We also acknowledge use of the photometric archival data from the Asteroid Terrestrial-impact Last Alert System (ATLAS) project. See (Tonry et al. 2018) and (Heinze et al. 2018) for specifics of the ATLAS survey.

This publication makes use of data products from the Wide-field Infrared Survey Explorer, which is a joint project of the University of California, Los Angeles, and the Jet Propulsion Laboratory/California Institute of Technology, funded by the National Aeronautics and Space Administration.

This publication makes use of data products from the Two Micron All Sky Survey, which is a joint project of the University of Massachusetts and the Infrared Processing and Analysis Center/California Institute of Technology, funded by the National Aeronautics and Space Administration and the National Science Foundation.

We used the Simbad service operated by the Centre des Données Stellaires (Strasbourg, France) and the ESO Science Archive Facility services (data obtained under request number 396301).

This research has made use of the VizieR catalogue access tool, CDS, Strasbourg, France (DOI : 10.26093/cds/vizie). The original description of the VizieR service was published in (Ochsenbein et al. 2000).

## DATA AVAILABILITY

The *TESS* data underlying this article were accessed from MAST (Barbara A. Mikulski Archive for Space Telescopes) Portal (<https://mast.stsci.edu/portal/Mashup/Clients/Mast/Portal.html>), including the data products found in the bulk download website ([http://archive.stsci.edu/tess/bulk\\_downloads/bulk\\_downloads\\_ffl-tp-1c-dv.html](http://archive.stsci.edu/tess/bulk_downloads/bulk_downloads_ffl-tp-1c-dv.html)). Part of the data were derived from sources in public domain as given in the respective footnotes. The derived data generated in this research and the code used for the photodynamical analysis will be shared on reasonable request to the corresponding author.

## REFERENCES

- Babusiaux C., et al., 2023, *A&A*, 674, A32  
 Bailer-Jones C. A. L., Rybizki J., Foesneau M., Demleitner M., Andrae R., 2021, *AJ*, 161, 147  
 Borkovits T., Csizmadia S., Hegedüs T., Bíró I. B., Sándor Z., Opitz A., 2002, *A&A*, 392, 895  
 Borkovits T., Forgács-Dajka E., Regály Z., 2004, *A&A*, 426, 951  
 Borkovits T., et al., 2013, *MNRAS*, 428, 1656  
 Borkovits T., Rappaport S., Hajdu T., Sztakovics J., 2015, *MNRAS*, 448, 946  
 Borkovits T., et al., 2018, *MNRAS*, 478, 5135  
 Borkovits T., et al., 2019a, *MNRAS*, 483, 1934  
 Borkovits T., Sperauskas J., Tokovinin A., Latham D. W., Csányi I., Hajdu T., Molnár L., 2019b, *MNRAS*, 487, 4631  
 Borkovits T., Rappaport S. A., Hajdu T., Maxted P. F. L., Pál A., Forgács-Dajka E., Klagyivik P., Mitnyan T., 2020a, *MNRAS*, 493, 5005  
 Borkovits T., et al., 2020b, *MNRAS*, 496, 4624  
 Borkovits T., et al., 2021, *MNRAS*, 503, 3759  
 Borkovits T., et al., 2022, *MNRAS*, 510, 1352  
 Borucki W. J., et al., 2010, *Science*, 327, 977  
 Bressan A., Marigo P., Girardi L., Salasnich B., Dal Cero C., Rubele S., Nanni A., 2012, *MNRAS*, 427, 127  
 Carter J. A., et al., 2011, *Science*, 331, 562  
 Choi J., Dotter A., Conroy C., Cantiello M., Paxton B., Johnson B. D., 2016, *ApJ*, 823, 102  
 Cutri R. M., et al., 2021, VizieR Online Data Catalog, p. II/328  
 Czavalinga D. R., Mitnyan T., Rappaport S. A., Borkovits T., Gagliano R., Omohundro M., Kristiansen M. H. K., Pál A., 2023, *A&A*, 670, A75  
 Deras A., et al., 2011, *Science*, 332, 216  
 Dotter A., 2016, *ApJS*, 222, 8  
 Fuller J., Deras A., Borkovits T., Huber D., Bedding T. R., Kiss L. L., 2013, *MNRAS*, 429, 2425  
 Gaia Collaboration 2022, VizieR Online Data Catalog, p. I/357  
 Gaia Collaboration et al., 2023, *A&A*, 674, A1  
 Gao Y., van Roestel J., Green M. J., Fuller J., Grishin E., Toonen S., 2023, *MNRAS*, 521, 2114  
 Hajdu T., Borkovits T., Forgács-Dajka E., Sztakovics J., Marschalkó G., Benkő J. M., Klagyivik P., Sallai M. J., 2017, *MNRAS*, 471, 1230  
 Hajdu T., Borkovits T., Forgács-Dajka E., Sztakovics J., Bódi A., 2022, *MNRAS*, 509, 246  
 Heinze A. N., et al., 2018, *AJ*, 156, 241  
 Henden A. A., Levine S., Terrell D., Welch D. L., 2015, in American Astronomical Society Meeting Abstracts #225, p. 336.16  
 Hippke M., David T. J., Mulders G. D., Heller R., 2019, *AJ*, 158, 143  
 Kiseleva L. G., Eggleton P. P., Mikkola S., 1998, *MNRAS*, 300, 292  
 Kochanek C. S., et al., 2017, *PASP*, 129, 104502  
 Kostov V. B., et al., 2021, *ApJ*, 917, 93  
 Kovács G., Zucker S., Mazeh T., 2002, *A&A*, 391, 369  
 Lightkurve Collaboration et al., 2018, Lightkurve: Kepler and TESS time series analysis in Python, Astrophysics Source Code Library (ascl:1812.013)  
 Marcussen M. L., Albrecht S. H., 2023, *AJ*, 165, 266  
 Mitnyan T., Borkovits T., Rappaport S. A., Pál A., Maxted P. F. L., 2020, *MNRAS*, 498, 6034  
 Ochsenbein F., Bauer P., Marcout J., 2000, *A&AS*, 143, 23  
 Paegert M., Stassun K. G., Collins K. A., Pepper J., Torres G., Jenkins J., Twicken J. D., Latham D. W., 2021, *arXiv e-prints*, p. arXiv:2108.04778

- Pál A., 2012, *MNRAS*, 421, 1825
- Pourbaix D., et al., 2022, Gaia DR3 documentation Chapter 7: Non-single stars, Gaia DR3 documentation, European Space Agency; Gaia Data Processing and Analysis Consortium. Online at <https://gea.esac.esa.int/archive/documentation/GDR3/index.html>, id. 7
- Powell B. P., et al., 2022, *ApJ*, 938, 133
- Rappaport S. A., et al., 2022, *MNRAS*, 513, 4341
- Rappaport S. A., et al., 2023, *MNRAS*, 521, 558
- Ricker G. R., et al., 2015, *Journal of Astronomical Telescopes, Instruments, and Systems*, 1, 014003
- Rowan D. M., et al., 2023, *MNRAS*, 520, 2386
- Shappee B. J., et al., 2014, *ApJ*, 788, 48
- Skrutskie M. F., et al., 2006, *AJ*, 131, 1163
- Smith K. W., et al., 2020, *PASP*, 132, 085002
- Southworth J., et al., 2011, *MNRAS*, 414, 2413
- Tonry J. L., et al., 2018, *PASP*, 130, 064505
- Tran K., Levine A., Rappaport S., Borkovits T., Csizmadia S., Kalomeni B., 2013, *ApJ*, 774, 81

## **APPENDIX A: MID-ECLIPSE TIMES OF THE FOUR ECLIPSING BINARIES**

This paper has been typeset from a  $\text{\TeX}/\text{\LaTeX}$  file prepared by the author.

**Table A1.** Times of minima of TIC 014839347.

BJD −2 400 000	Cycle no.	std. dev. ( <i>d</i> )	BJD −2 400 000	Cycle no.	std. dev. ( <i>d</i> )	BJD −2 400 000	Cycle no.	std. dev. ( <i>d</i> )	BJD −2 400 000	Cycle no.	std. dev. ( <i>d</i> )
58683.46208	−0.5	0.00036	58712.27472	24.5	0.00042	59422.20711	640.5	0.00022	59799.07319	967.5	0.00018
58684.04020	0.0	0.00009	58712.85171	25.0	0.00013	59422.78730	641.0	0.00008	59799.64946	968.0	0.00011
58684.61498	0.5	0.00123	58713.42656	25.5	0.00023	59423.36554	641.5	0.00029	59800.22534	968.5	0.00025
58685.19280	1.0	0.00020	58714.00445	26.0	0.00015	59423.94014	642.0	0.00010	59800.80247	969.0	0.00010
58685.76391	1.5	0.00036	58714.58008	26.5	0.00055	59424.51522	642.5	0.00027	59801.37868	969.5	0.00025
58686.34518	2.0	0.00019	58715.15689	27.0	0.00015	59425.09262	643.0	0.00013	59801.95434	970.0	0.00008
58686.92020	2.5	0.00063	58715.73324	27.5	0.00083	59425.66792	643.5	0.00026	59802.52871	970.5	0.00025
58687.49786	3.0	0.00028	58716.30855	28.0	0.00022	59426.24497	644.0	0.00015	59803.10674	971.0	0.00012
58688.07271	3.5	0.00060	58716.88273	28.5	0.00017	59426.82292	644.5	0.00034	59803.68408	971.5	0.00028
58688.64952	4.0	0.00012	58717.46216	29.0	0.00017	59427.39750	645.0	0.00013	59804.25859	972.0	0.00010
58689.22368	4.5	0.00056	58718.03791	29.5	0.00072	59427.97102	645.5	0.00047	59804.83306	972.5	0.00026
58689.80177	5.0	0.00023	58718.61384	30.0	0.00021	59428.55059	646.0	0.00011	59805.41148	973.0	0.00008
58690.37606	5.5	0.00056	58719.19201	30.5	0.00026	59429.12418	646.5	0.00041	59805.98763	973.5	0.00032
58690.95388	6.0	0.00014	58719.76702	31.0	0.00034	59431.43166	648.5	0.00018	59806.56397	974.0	0.00008
58691.52642	6.5	0.00044	58720.34276	31.5	0.00021	59432.00803	649.0	0.00008	59807.13972	974.5	0.00034
58692.10763	7.0	0.00021	58721.49532	32.5	0.00057	59432.58124	649.5	0.00161	59807.71629	975.0	0.00013
58692.67565	7.5	0.00170	58722.07231	33.0	0.00011	59433.73796	650.5	0.00120	59808.29119	975.5	0.00023
58693.83076	8.5	0.00055	58722.64775	33.5	0.00078	59434.31238	651.0	0.00008	59808.86828	976.0	0.00010
58694.41220	9.0	0.00016	58723.22456	34.0	0.00026	59434.88859	651.5	0.00034	59809.44182	976.5	0.00039
58694.98602	9.5	0.00039	58723.80602	34.5	0.00164	59435.46581	652.0	0.00009	59811.17408	978.0	0.00009
58695.56427	10.0	0.00012	58725.52948	36.0	0.00020	59436.04049	652.5	0.00027	59811.74866	978.5	0.00028
58696.13822	10.5	0.00063	58726.10307	36.5	0.00038	59436.61758	653.0	0.00009	59812.32618	979.0	0.00009
58697.86901	12.0	0.00018	58726.68231	37.0	0.00010	59437.19277	653.5	0.00041	59812.90057	979.5	0.00029
58698.44024	12.5	0.00036	58727.25884	37.5	0.00021	59437.76986	654.0	0.00010	59813.47942	980.0	0.00010
58699.02193	13.0	0.00017	58727.83522	38.0	0.00020	59438.34494	654.5	0.00028	59814.05354	980.5	0.00015
58699.59538	13.5	0.00079	58728.41084	38.5	0.00022	59438.92271	655.0	0.00013	59814.63170	981.0	0.00012
58700.17426	14.0	0.00015	58728.98760	39.0	0.00012	59439.49674	655.5	0.00031	59815.20384	981.5	0.00035
58700.75026	14.5	0.00052	58729.56338	39.5	0.00037	59440.07554	656.0	0.00021	59815.78414	982.0	0.00010
58701.32582	15.0	0.00015	58730.14071	40.0	0.00022	59440.65165	656.5	0.00023	59816.35846	982.5	0.00018
58701.90006	15.5	0.00019	58730.71633	40.5	0.00038	59441.22686	657.0	0.00011	59816.93536	983.0	0.00011
58702.47884	16.0	0.00018	58731.29283	41.0	0.00014	59441.80305	657.5	0.00041	59817.51193	983.5	0.00026
58703.05672	16.5	0.00099	58731.86939	41.5	0.00035	59442.37988	658.0	0.00011	59818.08789	984.0	0.00010
58704.20398	17.5	0.00257	58732.44572	42.0	0.00014	59442.95537	658.5	0.00028	59818.66672	984.5	0.00022
58704.78336	18.0	0.00015	58733.02129	42.5	0.00023	59443.53204	659.0	0.00013	59819.24122	985.0	0.00011
58705.35753	18.5	0.00045	58733.59824	43.0	0.00026	59444.10607	659.5	0.00036	59819.81796	985.5	0.00026
58705.93572	19.0	0.00020	58734.17401	43.5	0.00028	59444.68495	660.0	0.00009	59820.39417	986.0	0.00011
58706.50396	19.5	0.00117	58735.32918	44.5	0.00115	59445.25979	660.5	0.00027	59820.96853	986.5	0.00023
58707.67101	20.5	0.00074	58735.90361	45.0	0.00020	59445.83675	661.0	0.00011	59821.54589	987.0	0.00009
58708.24049	21.0	0.00018	58736.47388	45.5	0.00151	59446.41231	661.5	0.00025	59822.12237	987.5	0.00036
58708.81818	21.5	0.00024	59420.48162	639.0	0.00012	59797.34480	966.0	0.00009	59822.69894	988.0	0.00010
58709.39326	22.0	0.00023	59421.05827	639.5	0.00022	59797.91970	966.5	0.00024	59823.27240	988.5	0.00021
58709.96928	22.5	0.00051	59421.63472	640.0	0.00013	59798.49733	967.0	0.00012	59823.85117	989.0	0.00010
58711.69848	24.0	0.00020									

**Table A2.** Times of minima of TIC 066893949.

BJD −2 400 000	Cycle no.	std. dev. ( <i>d</i> )	BJD −2 400 000	Cycle no.	std. dev. ( <i>d</i> )	BJD −2 400 000	Cycle no.	std. dev. ( <i>d</i> )	BJD −2 400 000	Cycle no.	std. dev. ( <i>d</i> )
58711.83201	−0.5	0.00072	58733.46997	4.0	0.00018	59435.09934	150.0	0.00007	59802.71738	226.5	0.00018
58714.24737	0.0	0.00019	58735.85916	4.5	0.00032	59437.48807	150.5	0.00018	59805.13517	227.0	0.00009
58716.63577	0.5	0.00183	59420.68260	147.0	0.00009	59439.90506	151.0	0.00008	59812.33065	228.5	0.00020
58719.05333	1.0	0.00014	59423.06986	147.5	0.00019	59442.29382	151.5	0.00021	59814.74714	229.0	0.00007
58721.44275	1.5	0.00038	59425.48859	148.0	0.00008	59444.71088	152.0	0.00009	59817.13492	229.5	0.00022
58726.24731	2.5	0.00061	59427.87673	148.5	0.00015	59797.91148	225.5	0.00025	59819.55200	230.0	0.00010
58728.66411	3.0	0.00016	59430.29490	149.0	0.00009	59800.32911	226.0	0.00007	59821.93961	230.5	0.00027
58731.05216	3.5	0.00087									

**Table A3.** Times of minima of TIC 088206187.

BJD -2 400 000	Cycle no.	std. dev. ( <i>d</i> )	BJD -2 400 000	Cycle no.	std. dev. ( <i>d</i> )	BJD -2 400 000	Cycle no.	std. dev. ( <i>d</i> )	BJD -2 400 000	Cycle no.	std. dev. ( <i>d</i> )
58816.34459	-0.5	0.00033	58830.55929	11.5	0.00067	59914.20263	926.5	0.00017	59925.45387	936.0	0.00013
58816.93757	0.0	0.00079	58831.15198	12.0	0.00024	59914.79520	927.0	0.00011	59926.04698	936.5	0.00017
58817.53133	0.5	0.00045	58831.74569	12.5	0.00050	59915.38830	927.5	0.00015	59926.63933	937.0	0.00013
58818.12388	1.0	0.00049	58832.33502	13.0	0.00017	59915.97845	928.0	0.00012	59927.23320	937.5	0.00019
58818.71385	1.5	0.00093	58832.92766	13.5	0.00169	59916.57213	928.5	0.00020	59927.82292	938.0	0.00015
58819.30876	2.0	0.00018	58833.51975	14.0	0.00029	59917.16356	929.0	0.00012	59928.41569	938.5	0.00020
58819.90018	2.5	0.00084	58834.11457	14.5	0.00110	59917.75583	929.5	0.00020	59929.00834	939.0	0.00010
58820.49284	3.0	0.00025	58834.70346	15.0	0.00013	59918.34719	930.0	0.00010	59929.60009	939.5	0.00027
58821.08425	3.5	0.00207	58835.29747	15.5	0.00130	59918.93905	930.5	0.00018	59930.19175	940.0	0.00013
58821.67783	4.0	0.00035	58835.88897	16.0	0.00017	59919.53184	931.0	0.00010	59930.78609	940.5	0.00013
58822.26863	4.5	0.00045	58836.48139	16.5	0.00042	59920.12605	931.5	0.00022	59931.37704	941.0	0.00012
58822.86037	5.0	0.00021	58837.07319	17.0	0.00038	59920.71698	932.0	0.00012	59931.97030	941.5	0.00014
58823.45424	5.5	0.00038	58837.66618	17.5	0.00029	59921.30883	932.5	0.00022	59932.56131	942.0	0.00008
58824.04631	6.0	0.00062	58838.25782	18.0	0.00086	59921.90097	933.0	0.00009	59933.15368	942.5	0.00017
58824.63694	6.5	0.00056	58838.84976	18.5	0.00033	59922.49323	933.5	0.00016	59933.74530	943.0	0.00012
58825.22950	7.0	0.00024	58839.44051	19.0	0.00072	59923.08616	934.0	0.00015	59934.33831	943.5	0.00043
58825.82227	7.5	0.00021	58840.03120	19.5	0.00044	59924.27054	935.0	0.00015	59934.92946	944.0	0.00014
58826.41376	8.0	0.00018	58840.62481	20.0	0.00047	59924.86028	935.5	0.00025	59935.52280	944.5	0.00025
58827.00838	8.5	0.00043	59913.61059	926.0	0.00013						

**Table A4.** Times of minima of TIC 298714297.

BJD -2 400 000	Cycle no.	std. dev. ( <i>d</i> )	BJD -2 400 000	Cycle no.	std. dev. ( <i>d</i> )	BJD -2 400 000	Cycle no.	std. dev. ( <i>d</i> )	BJD -2 400 000	Cycle no.	std. dev. ( <i>d</i> )
58711.49994	0.0	0.00037	58737.24706	24.0	0.00024	59816.56348	1030.0	0.00007	59835.33955	1047.5	0.00009
58712.03597	0.5	0.00063	59797.25118	1012.0	0.00005	59817.09956	1030.5	0.00028	59835.87540	1048.0	0.00005
58712.57261	1.0	0.00040	59797.78710	1012.5	0.00022	59817.63617	1031.0	0.00018	59836.41296	1048.5	0.00011
58713.64553	2.0	0.00032	59798.32436	1013.0	0.00010	59818.17406	1031.5	0.00031	59836.94845	1049.0	0.00005
58714.18127	2.5	0.00043	59798.86084	1013.5	0.00022	59818.70930	1032.0	0.00007	59837.48540	1049.5	0.00014
58714.71826	3.0	0.00054	59799.93378	1014.5	0.00038	59819.24606	1032.5	0.00021	59838.02128	1050.0	0.00005
58715.79108	4.0	0.00017	59800.46966	1015.0	0.00015	59819.78208	1033.0	0.00019	59839.09430	1051.0	0.00004
58716.32573	4.5	0.00092	59801.00665	1015.5	0.00028	59820.31865	1033.5	0.00033	59839.63180	1051.5	0.00010
58716.86396	5.0	0.00038	59801.54269	1016.0	0.00007	59820.85502	1034.0	0.00008	59840.16712	1052.0	0.00004
58717.93698	6.0	0.00020	59802.07904	1016.5	0.00047	59821.39111	1034.5	0.00019	59840.70440	1052.5	0.00011
58718.47299	6.5	0.00059	59802.61562	1017.0	0.00015	59821.92778	1035.0	0.00019	59841.24016	1053.0	0.00005
58719.00964	7.0	0.00038	59803.15228	1017.5	0.00020	59822.46474	1035.5	0.00025	59841.77669	1053.5	0.00010
58720.08276	8.0	0.00044	59803.68825	1018.0	0.00009	59823.00079	1036.0	0.00008	59842.31323	1054.0	0.00004
58720.61764	8.5	0.00054	59804.76143	1019.0	0.00010	59823.53781	1036.5	0.00035	59842.84990	1054.5	0.00009
58721.15530	9.0	0.00040	59805.29855	1019.5	0.00022	59824.07355	1037.0	0.00036	59843.38607	1055.0	0.00005
58722.22824	10.0	0.00009	59805.83441	1020.0	0.00013	59825.68383	1038.5	0.00014	59843.92310	1055.5	0.00009
58722.76369	10.5	0.00080	59806.37126	1020.5	0.00031	59826.21946	1039.0	0.00005	59844.45912	1056.0	0.00006
58723.30097	11.0	0.00042	59806.90729	1021.0	0.00014	59826.75659	1039.5	0.00011	59844.99635	1056.5	0.00011
58725.44656	13.0	0.00025	59807.44376	1021.5	0.00027	59827.29228	1040.0	0.00004	59845.53190	1057.0	0.00004
58726.51958	14.0	0.00009	59807.98022	1022.0	0.00005	59827.82956	1040.5	0.00014	59846.60491	1058.0	0.00005
58727.05501	14.5	0.00107	59808.51656	1022.5	0.00020	59828.36514	1041.0	0.00005	59847.14169	1058.5	0.00016
58727.59211	15.0	0.00019	59809.05307	1023.0	0.00018	59828.90253	1041.5	0.00012	59847.67775	1059.0	0.00005
58728.66521	16.0	0.00011	59809.58973	1023.5	0.00030	59829.43803	1042.0	0.00005	59848.21495	1059.5	0.00010
58729.20005	16.5	0.00225	59811.19906	1025.0	0.00014	59829.97538	1042.5	0.00012	59848.75079	1060.0	0.00004
58729.73778	17.0	0.00018	59811.73565	1025.5	0.00027	59830.51100	1043.0	0.00005	59849.28744	1060.5	0.00014
58730.81024	18.0	0.00046	59812.27176	1026.0	0.00008	59831.04834	1043.5	0.00010	59849.82361	1061.0	0.00005
58731.34656	18.5	0.00033	59812.80619	1026.5	0.00019	59831.58384	1044.0	0.00006	59850.36021	1061.5	0.00009
58731.88324	19.0	0.00004	59813.34481	1027.0	0.00016	59832.12125	1044.5	0.00013	59850.89676	1062.0	0.00005
58732.95598	20.0	0.00039	59813.88129	1027.5	0.00019	59832.65671	1045.0	0.00005	59851.43322	1062.5	0.00016
58734.02900	21.0	0.00009	59814.41770	1028.0	0.00007	59833.19406	1045.5	0.00010	59851.96958	1063.0	0.00004
58735.10149	22.0	0.00046	59814.95407	1028.5	0.00022	59833.72953	1046.0	0.00004	59852.50629	1063.5	0.00010
58735.63702	22.5	0.00033	59815.49060	1029.0	0.00020	59834.26648	1046.5	0.00013	59853.04255	1064.0	0.00007
58736.17434	23.0	0.00002	59816.02711	1029.5	0.00026	59834.80254	1047.0	0.00005			